Geol. Mag. **148** (*1*), *2011, pp. 133–153. © Cambridge University Press 2010*
doi:10.1017/S0016756810000518

Carbon- and oxygen-isotope records of palaeoenvironmental and carbonate production changes in shallow-marine carbonates (Kimmeridgian, Swiss Jura)

CLAUDE COLOMBIÉ*†, CHRISTOPHE LÉCUYER* & ANDRÉ STRASSER‡

*UMR CNRS 5125 PEPS, Université Lyon 1, La Doua, bâtiment Géode, F-69622, Villeurbanne cedex, France
‡Department of Geosciences, Chemin du Musée 6, University of Fribourg, 1700 Fribourg, Switzerland

(*Received* 27 July 2009; *accepted* 14 April 2010; *first published online* 2 July 2010)

Abstract – Carbon- and oxygen-isotope ratios are commonly used to correlate shallow- and deep-marine successions. Carbon- and oxygen-isotope analyses were performed on bulk-carbonate samples from two Kimmeridgian sections of the Swiss Jura platform in order to correlate them with biostratigraphically well-dated coeval sections in the adjacent basin. On the platform, a general decrease in $\delta^{13}C$ and $\delta^{18}O$ values from the base to the top of the studied interval is measured, whereas time-equivalent pelagic–hemipelagic carbonates record an increase in carbon- and oxygen-isotope ratios. Moreover, the measured $\delta^{13}C$ and $\delta^{18}O$ values are generally lower than those indicated for the Kimmeridgian open ocean and show high-frequency variations superimposed on the general trend. Samples were screened for diagenetic alteration using optical and cathodoluminescence petrography and coupled carbon- and oxygen-isotope and trace-element analyses. Some observations favour a role for diagenetic alteration, but isotopic and elemental trends as well as sedimentological evidence suggest that the more negative values of $\delta^{13}C$ and $\delta^{18}O$ relative to Kimmeridgian seawater are also due to local environmental conditions. High-frequency changes in $\delta^{18}O$ and $\delta^{13}C$ values most likely result from variations in salinity and carbonate production and accumulation rates. These variations were produced by different water masses that were isolated from the open ocean and developed their own geochemical signatures. Repeated isolation was induced by high-frequency sea-level fluctuations and helped by irregular platform morphology. Consequently, carbon- and oxygen-isotope records in shallow-marine carbonates can be used for stratigraphic correlation only if their origin is well known.

Keywords: stable isotopes, Kimmeridgian, Swiss Jura Mountains, palaeoenvironmental parameters, carbonate production.

1. Introduction

Many shallow-marine carbonates do not preserve a simple geochemical record of their depositional environment because the sediments are commonly exposed to meteoric water before they have reached mineralogical stability (Allan & Matthews, 1982). Diagenetic stabilization of the carbonate constituents is accompanied by concomitant textural and chemical changes (Brand & Veizer, 1980, 1981). Notably, bulk matrix $\delta^{13}C$ data cannot be considered to be free of diagenetic artefacts (Immenhauser, Holmden & Patterson, 2007). For example, Immenhauser *et al.* (2003) explained local positive shifts in carbonate $\delta^{13}C$ and $\delta^{18}O$ values in a thick carbonate platform succession of Palaeozoic strata by geochemically altered platform-top water masses and the effects of early meteoric diagenesis. Furthermore, Patterson & Walter (1994*a*) showed that seawater ΣCO_2 from modern carbonate platforms (Bahama Banks and Florida) is depleted in ^{13}C by as much as 4 ‰ relative to open-ocean water. Similarly, Joachimski (1994) showed that Purbeckian peritidal micrites deposited in different depositional environments display distinct, facies-dependent carbon-isotope ratios. Therefore, shallow-marine carbonates may develop their own isotopic signature that depends mainly on early meteoric diagenesis and local palaeoenvironmental parameters. However, an increasing number of studies note a correlation of $\delta^{13}C$ values between shallow-water and deep-water successions. These studies have lent further support to the applicability of $\delta^{13}C$ variations in shallow-marine carbonates for stratigraphic purposes (Immenhauser *et al.* 2003; Buonocunto *et al.* 2002; Glumac & Walker, 1998; Grötsch, Billing & Vahrenkamp, 1998; Immenhauser *et al.* 2002; Krull *et al.* 2004; Magaritz, 1983; Marshall & Middleton, 1980; Swart & Eberli, 2005; Vahrenkamp, 1996; Weissert *et al.* 1998).

Generally, the Kimmeridgian (Late Jurassic) can be considered as a greenhouse period (Hallam, 1985; Sellwood, Valdes & Price, 2000). In the Swiss Jura, sedimentological and clay-mineralogical analyses of shallow-marine carbonates indicate that climate changed from more humid to more arid at the boundary between the Early and Late Kimmeridgian (Colombié, 2002). This result is consistent with the findings of several authors (Abbink *et al.* 2001; Hallam, 1984; Price, 1999; Rameil, 2005; Wignall & Ruffell, 1990), who have indicated a drier phase towards the

†Author for correspondence: claude.colombie@univ-lyon1.fr

Jurassic/Cretaceous boundary (from the Kimmeridgian to the Early Berriasian). The Late Kimmeridgian was the end of a second-order transgression that started in the Late Oxfordian (Hardenbol *et al.* 1998). Despite this transgression, the Kimmeridgian of the Swiss Jura contains bioturbated mudstones with circum-granular cracks, desiccation cracks, tepees or fenestrae that indicate low-energy depositional environments between the upper intertidal and supratidal zones (Colombié & Strasser, 2005). This implies that carbonate productivity was such that the platform could keep up with sea-level rise and even outpace it. However, there is not any sedimentary evidence of repeated and prolonged emergence (e.g. gravitational cements, vadose pisoids, alveolar structures, dissolution vugs, recrystallization of micritic matrix, or rootlet structures). These shallow-water carbonates therefore have a high potential for the preservation of the primary oxygen- and carbon-isotopic compositions.

The biostratigraphy of the Kimmeridgian of the Swiss Jura platform is only poorly defined. A high-resolution sequence-stratigraphic correlation with three biostratigraphically well-dated hemipelagic and pelagic sections located in the Vocontian Basin in France has been performed (Colombié & Strasser, 2003, 2005). The impetus for the present work was to constrain this correlation by using carbon and oxygen isotopes for correlation between the Kimmeridgian of the Swiss Jura and well-dated coeval sections in other western European basins. Carbon- and oxygen-isotope analyses were made from bulk-rock samples from two Kimmeridgian sections of the Swiss Jura platform. The obtained variations in $\delta^{13}C$ and $\delta^{18}O$ values correlate with changes in relative sea level. However, these isotopic records differ from those obtained from the same interval in other basins. The obtained values were also compared with the $\delta^{13}C$ and $\delta^{18}O$ values from coeval nonluminescent belemnite rostra and brachiopods measured in previous studies (Prokoph, Shields & Veizer, 2008; Riboulleau *et al.* 1998; Veizer *et al.* 1999; Wierzbowski, 2004), in order to identify the global versus local palaeoceanographic effects. Optical and cathodoluminescence petrography, as well as trends in elemental and isotopic data, were used in order to characterize the influence of meteoric diagenesis. Lastly, the $\delta^{13}C$ and $\delta^{18}O$ values were compared with the sedimentological and sequence-stratigraphical interpretation of the two studied sections (Colombié, 2002; Colombié & Strasser, 2005) in order to specify the origin of the isotopic record in the Kimmeridgian shallow-water carbonates of the Swiss Jura.

2. Geological context

Two Kimmeridgian platform sections, Gorges du Pichoux and Péry-Reuchenette, were studied to investigate their stable-isotope and trace-element compositions. They are located north of Biel in the central Swiss Jura (Fig. 1). During the Kimmeridgian,

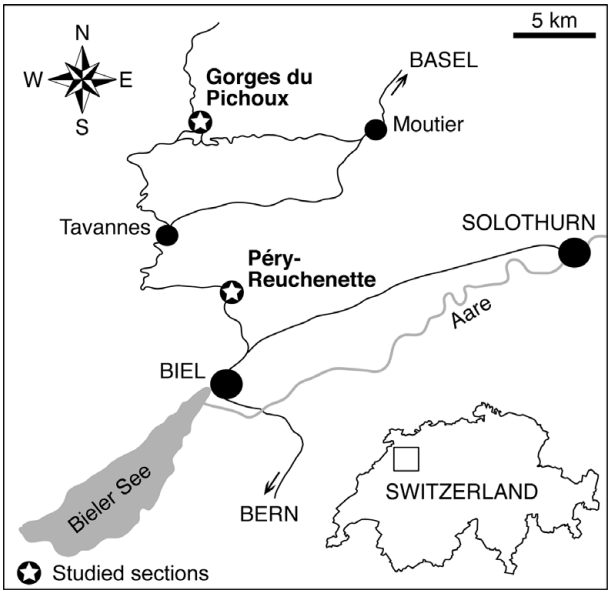

Figure 1. Geographical location of the studied sections. The Gorges du Pichoux section is in a more proximal position on the Jura platform than the Péry-Reuchenette section, and generally displays more restricted facies.

the Jura Mountains were a SW–NE-trending shallow carbonate platform located between the Paris Basin in the northwest and the Tethys Ocean in the southeast. The Gorges du Pichoux section, which is located north–northwest of the Péry-Reuchenette section, is in a more proximal position and displays generally more restricted facies. Nevertheless, both of the studied successions essentially include bioturbated mudstones and wackestones with moderate fossil diversity (ostracodes, bivalves, gastropods, miliolids, other benthic foraminifera, dasycladaceans and sponge spicules), which indicate semi-restricted lagoons (Colombié & Strasser, 2005). Such lime mudstones exhibit high porosities but low permeabilities (Enos & Sawatsky, 1981) that allow only minor pore-water flow. Residence time of waters within these semi-restricted lagoons was long because of weak exchange with open-ocean waters.

In the central Swiss Jura, the Kimmeridgian corresponds to the Reuchenette Formation (Gygi, 1995; Thalmann, 1966). The Reuchenette Formation lies between the white oolitic limestones of the Late Oxfordian Verena Member and the Early Tithonian 'Calcaires en Plaquettes' (Fig. 2). The ammonites of the Swiss Jura have a Tethyan affinity in the Early Kimmeridgian, while they suggest boreal influences in the Late Kimmeridgian (Gygi, 1995; Colombié & Rameil, 2007). The top of the Verena Member belongs to the upper part of the Planula ammonite zone (Gygi & Persoz, 1986). The upper boundary of the Reuchenette Formation corresponds to the top of the boreal Beckeri zone, which coincides with the Tethyan Autissiodorensis zone (Gygi, 1995; Meyer & Pittman, 1994). Sedimentological and sequence analyses of the Gorges du Pichoux and Péry-Reuchenette sections

https://doi.org/10.1017/S0016756810000518 Published online by Cambridge University Press

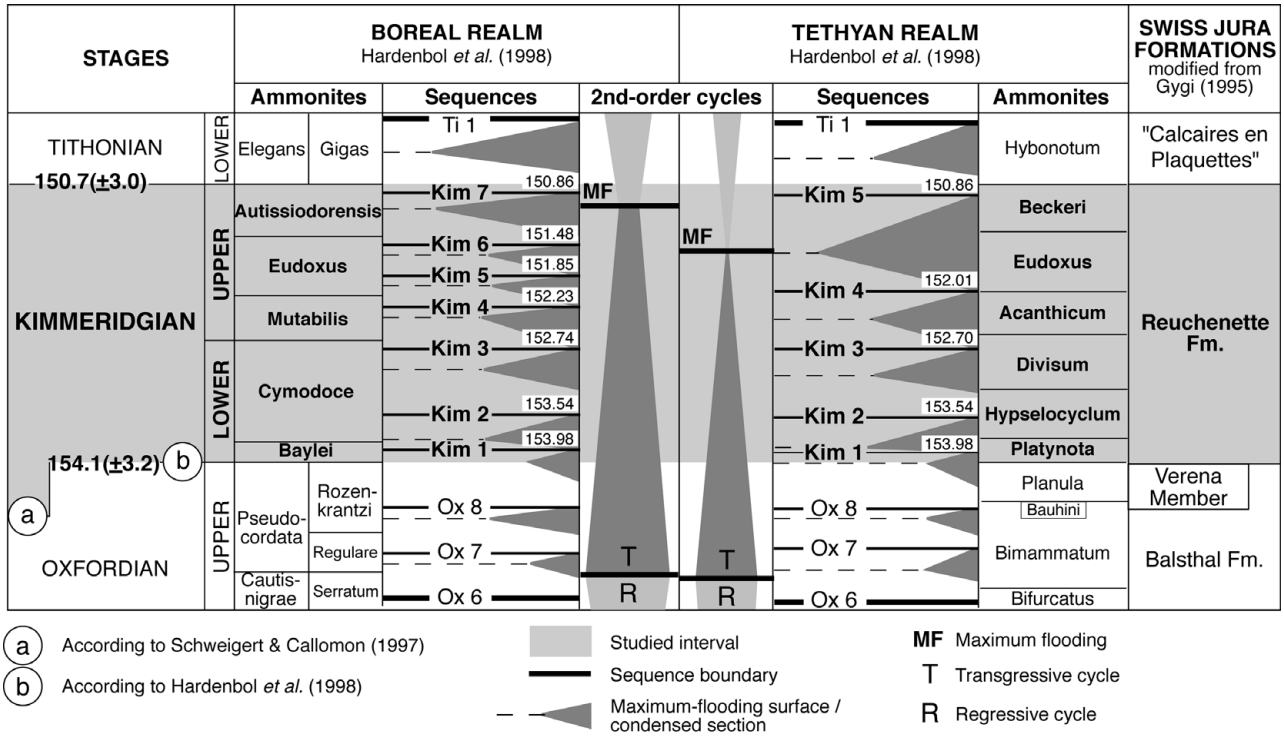

Figure 2. Stratigraphic chart for the studied interval and associated formations in the Swiss Jura. The most important increase in accommodation space in the Swiss Jura occurs in the Eudoxus ammonite zone, and coincides with the second-order maximum flooding defined by Hardenbol *et al.* (1998) for the Tethyan realm.

allow the definition of small-, medium- and large-scale depositional sequences that are hierarchically stacked. This hierarchy partly reflects the sedimentary record of climatic and sea-level changes that were in tune with the orbital (Milankovitch) cycles: the small-scale sequences correspond to the 100 ka short eccentricity cycle and the medium-scale sequences to the 400 ka long eccentricity cycle. Large-scale sequences are composed of two to three medium-scale sequences (Fig. 3; Colombié, 2002; Colombié & Strasser, 2005). The high-resolution sequence-stratigraphic correlation with three biostratigraphically well-dated hemipelagic and pelagic sections located in the Vocontian Basin in France allows a better definition of the chronostratigraphic framework (Colombié & Strasser, 2003, 2005). The most important increase in accommodation space in the Kimmeridgian of the Swiss Jura occurs in the Eudoxus ammonite zone (Late Kimmeridgian) and coincides with the end of the second-order transgression (that is, the second-order maximum flooding) defined by Hardenbol *et al.* (1998) for the Tethyan realm (Fig. 2). The platform-to-basin correlation also shows that the composition of hemipelagic and pelagic deposits depends, to a large extent, on cyclical variations of carbonate production in shallow-marine environments and subsequent export of carbonate mud to the basin (Colombié & Strasser, 2003). The most important increase in accommodation space in the Kimmeridgian of the Swiss Jura corresponds to the greatest increase in carbonate production and accumulation on the platform and export to the basin. Carbonate production on the platform generally outpaced accommodation gain. Consequently, despite the second-order maximum flooding that characterized the Late Kimmeridgian, the Swiss Jura platform was prograding (Colombié & Strasser, 2005).

3. Sampling and methods

Carbon- and oxygen-isotopic analyses were carried out on bulk carbonate samples from the Gorges du Pichoux and Péry-Reuchenette sections (Fig. 3). In the Gorges du Pichoux section, the whole Kimmeridgian was analysed, whereas the studied interval in the Péry-Reuchenette section includes the upper part of the Early Kimmeridgian and the lower part of the Late Kimmeridgian. Seventy-three samples from the Gorges du Pichoux section (2 or 3 metre sampling increments) and 65 samples from the Péry-Reuchenette section (1 or 2 metre sampling increments) were analysed. In order to reduce the effects of mineralogical and biological fractionations as well as diagenetic processes, fine-grained and texturally uniform matrix micrites from the deepest and most open-marine environments were sampled.

Fifty-four analyses from the Gorges du Pichoux section were performed with a VG Prism mass spectrometer at the ETH of Zurich (Switzerland). Then, 62 samples from the Péry-Reuchenette section and 3 samples from the Gorges du Pichoux section were analysed with a VG Prism series 2 at the Department of Earth Sciences of the University of Oxford (United Kingdom). Standard deviations in the Péry-Reuchenette samples are 0.03 ‰ for carbon and

https://doi.org/10.1017/S0016756810000518 Published online by Cambridge University Press

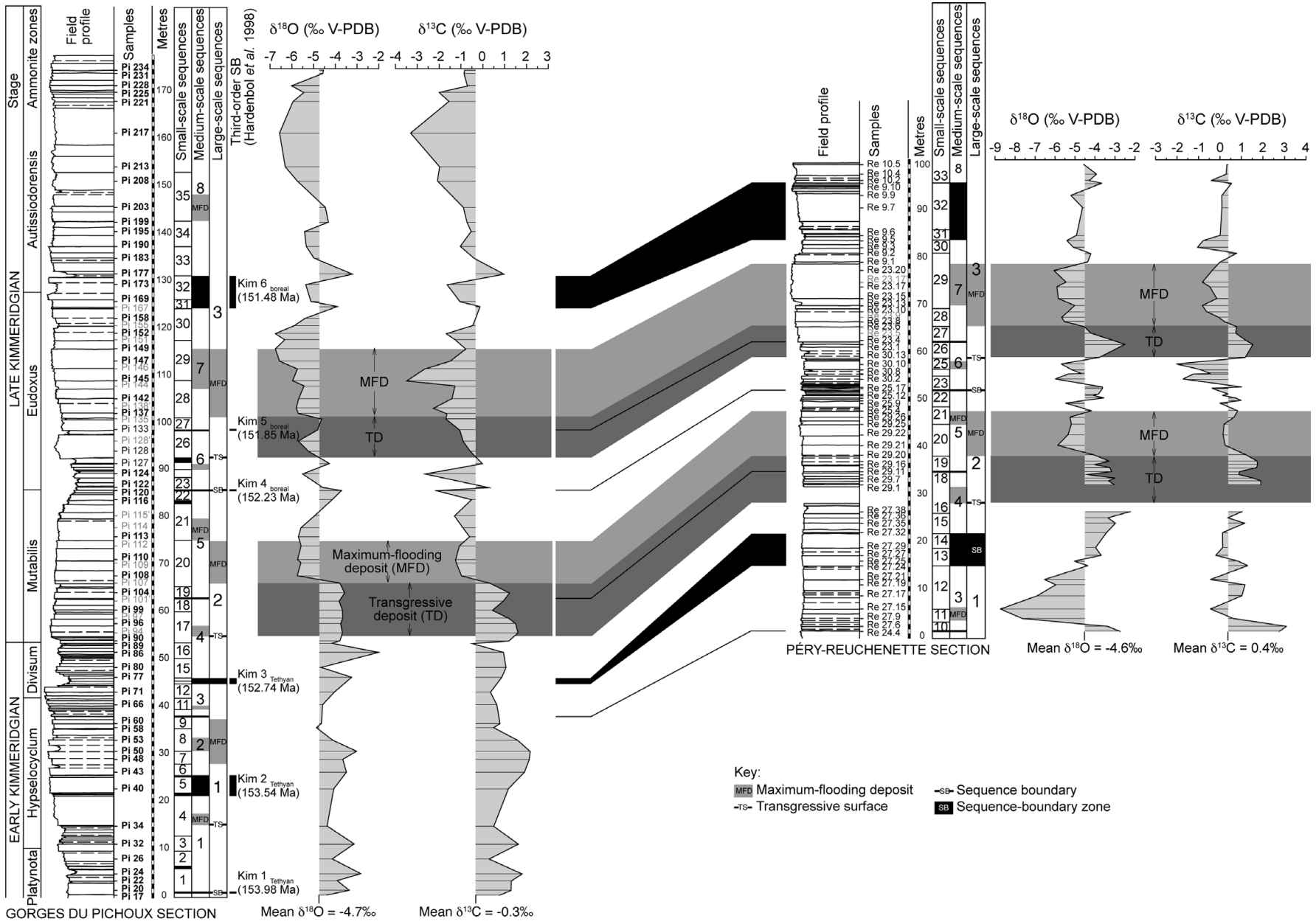

Figure 3. Correlation of oxygen- and carbon-isotope ratios between the Gorges du Pichoux and the Péry-Reuchenette sections, and comparison with the sequence-stratigraphic interpretation. Samples listed in bold type were analysed in Zurich, those in regular type in Oxford, those in grey in Lyon. In each section, changes in $\delta^{18}O$ resemble those in $\delta^{13}C$. Moreover, variations in oxygen- and carbon-isotopic composition in the Gorges du Pichoux section are similar to those in the Péry-Reuchenette section. Lastly, both studied sections record a general decrease in the oxygen- and carbon-isotope ratios from the base to the top of the studied interval, on which high-resolution changes in $\delta^{18}O$ and $\delta^{13}C$ values are superimposed.

0.09 to 0.1 ‰ for oxygen, while they are 0.06 ‰ for carbon and 0.1 ‰ for oxygen in the Gorges du Pichoux samples. Isotopic results are reported in per mil deviation from the V-PDB (Vienna Pee Dee Belemnite) using the standard delta notation. Lastly, 16 samples from the Gorges du Pichoux section and 3 samples from the Péry-Reuchenette section were analysed with a GV Instruments MultiPrep carbonate preparation device directly coupled to a GV Instruments IsoPrime mass spectrometer at the UMR CNRS 5125 of the University of Lyon 1 (France). Precision is better than 0.03 ‰ for carbon and 0.09 ‰ for oxygen.

Parallel to carbon- and oxygen-isotopic analyses, Sr, Mg, Na, Fe and Mn contents in bulk carbonate samples from the Gorges du Pichoux and Péry-Reuchenette sections were measured. The sampling procedure was the same as the one followed for carbon- and oxygen-isotope analyses. Then, around 15 g of rock were washed in demineralized water, dried in an oven at 80 °C, and powdered very finely. Fifty-five samples from the Gorges du Pichoux were analysed at the University of Dijon. Trace element concentrations in the carbonate fraction (acetic acid soluble fraction) were measured by atomic mass spectrophotometry following the standard procedure developed by Renard & Blanc (1971) and Richebois (1990). Sixty-two samples from the Péry-Reuchenette section were analysed at the Department of Earth Sciences of the University of Oxford. There, 40 mg of powder were dissolved in 1 mol/l acetic acid. The resulting sample solution was centrifuged to remove the residual phase. After adding an internal standard to the sample solution, it was diluted for the ICP mass spectrometer using 1 % HNO_3.

Stable-isotope and trace-element compositions were compared to each other (for different time intervals) by using reduced major axis (RMA) linear fitting (Davis, 2002). Scatter diagrams include statistical results. For each couple of variables, we calculated the Pearson correlation coefficient (r) in order to estimate the overall quality of the linear relations (the closer to ± 1, the better the linear relation). A significance t-test associated with this correlation coefficient indicates how far the sampled data are from the null hypothesis (H_0) of no linear relationship between the two variables. A low p-value (classically, < 0.05) refers to couples of variables whose linear relationship cannot be explained by sampling chance. Scatter diagrams include the estimated RMA lines only in this case. However, the correlation of time series of stable-isotope or trace-element compositions can be affected by time-autocorrelation effects. Estimating and testing for significance correlations calculated between time-differentiated variables (e.g. $\delta^{18}O_{t+1} - \delta^{18}O_t$ and $\delta^{13}C_{t+1} - \delta^{13}C_t$) can easily eliminate this problem. Still, significant correlation between such differentiated variables indicates that the correlation between the two original variables is not a spurious artefact of time-autocorrelation. An analysis of covariance (ANCOVA; Sokal & Rohlf, 1995) was performed in order to test for significance the null hypothesis that a same $\delta^{13}C$ versus $\delta^{18}O$ linear relation model holds for the various depositional environments, that is, that all the estimated regression lines are statistically equivalent. Here, a low p-value (classically, < 0.05) indicates that the compared samples actually refer to two or more distinct sets of linear relations. We further investigated the relationship between the ranked depositional environments along a more open-marine to more restricted gradient and the linear regression intercepts used for the ANCOVA (that is, the $\delta^{18}O$-values predicted by the sampled linear models for $\delta^{13}C = 0$). We used the Kendall rank correlation coefficient (τ) and its associated significance test (H_0: $\tau = 0$) (Abdi, 2007; Kendall & Gibbons, 1990). Kendall's τ is a robust (nonparametric) measure for nonlinear but monotonous relationship between two variables (the closer to ± 1, the stronger the correspondence between the two sets of ranked values).

Ten thin-sections from the Gorges du Pichoux were investigated with cathodoluminescence microscopy (CL MK3a, 17 kV gun voltage, 450 μA gun current). They are located below, in and above the transgressive and maximum-flooding deposits of the second and third large-scale sequences (Fig. 3).

4. Results

Results of the carbon- and oxygen-isotopic analyses from the Gorges du Pichoux and Péry-Reuchenette sections are plotted in Figure 3 and listed in Table 1. In the Gorges du Pichoux section, $\delta^{13}C$ and $\delta^{18}O$ values fluctuate to a large part in covariance and generally resemble those from the Péry-Reuchenette section (Fig. 3). Carbon- and oxygen-isotope values in the Gorges du Pichoux section range from -3.5 to 2.2 ‰ and from -6.7 to -2 ‰, respectively (Table 1). The mean values are -0.3 ± 1.4 ‰ for $\delta^{13}C$ and -4.7 ± 1.1 ‰ for $\delta^{18}O$. The lowest $\delta^{13}C$ and $\delta^{18}O$ values from the Péry-Reuchenette section are -2 ‰ and -8.7 ‰, respectively; the highest values are 3.1 ‰ and -2.2 ‰. The mean $\delta^{13}C$ and $\delta^{18}O$ values are 0.4 ± 1 ‰ and -4.6 ± 1.2 ‰, respectively. In both the Gorges du Pichoux and Péry-Reuchenette sections, the deviation from the mean value to the lowest value and highest value is at least one order greater than the standard deviation, indicating that fluctuations in $\delta^{13}C$ and $\delta^{18}O$ values are meaningful. $\delta^{13}C$ and $\delta^{18}O$ values generally decrease from the base to the top of both studied sections. Most $\delta^{13}C$ and $\delta^{18}O$ values are higher than the mean value in the lower part of the studied interval, whereas most of them are lower than the mean value in the upper part. The mean $\delta^{13}C$ and $\delta^{18}O$ values are lower at Gorges du Pichoux, which is the more proximal section, than at Péry-Reuchenette. The standard deviations for $\delta^{13}C$ and $\delta^{18}O$ values in the Gorges du Pichoux section are higher than those in the Péry-Reuchenette section.

Moreover, ($\delta^{13}C$, $\delta^{18}O$) scatter diagrams for the Gorges du Pichoux and Péry-Reuchenette sections

https://doi.org/10.1017/S0016756810000518 Published online by Cambridge University Press

Table 1. Carbon- and oxygen-isotope ratios (‰ V-PDB) from the Gorges du Pichoux (samples Pi) and Péry-Reuchenette (samples Re) sections

Samples	$\delta^{13}C$	$\delta^{18}O$	Samples	$\delta^{13}C$	$\delta^{18}O$	Samples	$\delta^{13}C$	$\delta^{18}O$	Samples	$\delta^{13}C$	$\delta^{18}O$	Samples	$\delta^{13}C$	$\delta^{18}O$
Gorges du Pichoux														
Pi 17	0.8	−4.4	**Pi 77**	0.9	−3.2	**Pi 113**	−0.6	−5.7	**Pi 145**	−3.5	−6.0	**Pi 203**	−0.9	−4.4
Pi 20	1.3	−3.3	**Pi 80**	1.1	−4.6	*Pi 114*	−0.9	−5.6	*Pi 146*	−2.7	−5.7	**Pi 208**	−2.1	−5.7
Pi 22	1.3	−3.9	**Pi 86**	1.0	−2.0	*Pi 115′*	−1.3	−4.9	**Pi 147**	−1.5	−6.5	**Pi 213**	−2.0	−6.3
Pi 24	1.8	−2.8	**Pi 89**	−0.5	−4.1	**Pi 116**	−0.5	−4.1	**Pi 149**	−0.8	−6.7	**Pi 217**	−3.3	−6.6
Pi 26	0.3	−4.1	**Pi 90**	1.2	−3.8	**Pi 120**	−2.1	−3.7	*Pi 151*	−1.2	−6.3	**Pi 221**	−1.5	−5.9
Pi 32	1.6	−3.1	*Pi 94*	1.6	−3.7	**Pi 122**	0.3	−4.6	**Pi 152**	−1.7	−6.7	**Pi 225**	−2.0	−5.4
Pi 34	0.5	−4.4	**Pi 96**	1.5	−3.7	**Pi 124**	−2.6	−5.5	*Pi 155*	−0.4	−5.9	**Pi 228**	−0.7	−6.0
Pi 40	1.2	−4.1	*Pi 97*	1.2	−3.6	Pi 127	0.0	−4.3	**Pi 158**	−0.3	−5.4	**Pi 231**	−0.8	−4.6
Pi 43	1.9	−3.5	**Pi 99**	0.4	−3.7	Pi 128	−0.6	−5.2	*Pi 167*	−0.1	−3.9	**Pi 234**	−0.8	−4.5
Pi 48	2.1	−3.6	*Pi 101′*	0.9	−3.8	*Pi 128′*	−0.9	−5.7	**Pi 169**	−1.0	−5.1			
Pi 50	2.2	−3.0	**Pi 104**	1.2	−3.6	Pi 133	−1.0	−4.8	**Pi 173**	−1.6	−5.3	Minimum	−3.5	−6.7
Pi 53	1.6	−4.1	*Pi 107*	0.3	−3.8	*Pi 135*	−1.7	−4.6	**Pi 177**	1.0	−3.2	Maximum	2.2	−2.0
Pi 58	0.5	−4.9	**Pi 108**	−1.0	−5.7	**Pi 137**	−1.6	−5.7	**Pi 183**	−0.4	−5.0	Mean	−0.3	−4.7
Pi 60	0.8	−4.6	*Pi 109*	−1.2	−5.6	*Pi 138′*	−2.2	−5.8	**Pi 190**	−1.0	−5.3	σ	1.4	1.1
Pi 66	0.7	−4.6	**Pi 110**	−1.2	−5.7	**Pi 142**	−1.4	−5.7	**Pi 195**	−0.5	−5.4			
Pi 71	0.4	−4.0	*Pi 112*	−1.1	−5.6	*Pi 144*	−1.3	−5.4	**Pi 199**	−0.7	−4.3			
Péry-Reuchenette														
Re 24.4	2.8	−2.7	Re 27.38	1.0	−2.2	Re 25.4	0.8	−4.2	Re 23.1	1.5	−2.5	Re 9.3	−1.0	−5.1
Re 27.6	3.1	−3.4	Re 29.1	1.9	−3.0	Re 25.9	0.0	−5.5	Re 23.4	1.2	−3.1	Re 9.5	−0.8	−5.4
Re 27.9	0.6	−7.6	Re 29.5	1.9	−3.3	Re 25.11	1.0	−4.5	*Re 23.5*	0.7	−4.2	Re 9.6	0.0	−4.9
Re 27.15	−0.4	−8.7	Re 29.7	1.5	−3.0	Re 25.12	0.7	−3.6	Re 23.6	0.8	−4.5	Re 9.7	0.1	−4.6
Re 27.17	1.0	−6.9	Re 29.9	0.9	−4.4	Re 25.14	0.1	−4.1	Re 23.8	0.2	−5.5	Re 9.9	0.1	−5.2
Re 27.19	1.2	−6.0	Re 29.11	0.9	−3.2	Re 25.15	0.4	−3.8	*Re 23.9′*	−0.1	−5.7	Re 9.10	0.5	−3.7
Re 27.21	−0.4	−6.5	Re 29.13	1.7	−3.3	Re 25.17	−0.4	−3.6	Re 23.10	−0.6	−5.3	Re 10.2	−0.4	−4.3
Re 27.24	1.3	−4.4	Re 29.16	1.7	−4.0	Re 25.18	1.0	−3.6	Re 23.13	−0.8	−5.0	Re 10.4	0.3	−3.9
Re 27.25	0.8	−5.0	Re 29.17	1.7	−3.3	Re 30.2	−1.7	−6.0	Re 23.15	−0.1	−5.8	Re 10.5	0.3	−4.6
Re 27.27	−0.2	−3.7	Re 29.20	1.2	−4.0	Re 30.5	−1.2	−5.3	Re 23.17	−0.5	−5.9			
Re 27.29	0.1	−4.0	Re 29.21	0.2	−5.9	Re 30.6	−0.4	−4.7	*Re 23.17′*	−0.8	−5.5	Minimum	−2.0	−8.7
Re 27.32	0.1	−3.4	Re 29.22	0.1	−5.3	Re 30.8	−0.9	−5.2	Re 23.20	−0.4	−6.1	Maximum	3.1	−2.2
Re 27.35	1.2	−3.0	Re 29.25	0.2	−5.2	Re 30.10	−2.0	−5.7	Re 9.1	0.0	−4.4	Mean	0.4	−4.6
Re 27.36	0.4	−3.4	Re 29.26	0.7	−5.2	Re 30.13	1.2	−3.8	Re 9.2	0.8	−4.2	σ	1.0	1.2

Samples in bold type were analysed in Zurich, those in regular type in Oxford, those in italic type in Lyon. σ is standard deviation.

show that carbon- and oxygen-isotope ratios behave as interrelated variables when including the whole studied interval or when looking only at its lower or upper part where most $\delta^{13}C$ and $\delta^{18}O$ values are higher or lower than the mean values, respectively (Fig. 4).

The comparison between the stable isotope records and the sequence-stratigraphical interpretation reveals high-frequency $\delta^{13}C$ and $\delta^{18}O$ changes: (1) $\delta^{13}C$ and $\delta^{18}O$ values that are higher than the mean values in the transgressive deposit (TD) of the second large-scale sequence; (2) $\delta^{13}C$ and $\delta^{18}O$ values that are lower than the mean values in the maximum-flooding deposit (MFD) of the second large-scale sequence; (3) a positive shift in $\delta^{13}C$ and $\delta^{18}O$ values in the TD of the third large-scale sequence in the Péry-Reuchenette section but a coeval negative shift in the Gorges du Pichoux section; and (4) a negative shift in $\delta^{13}C$ and $\delta^{18}O$ values in the MFD of the third large-scale sequence (Fig. 3). The main excursions discussed here are defined by numerous data points and are not the effects of simply one or a few samples deviating from the mean. The highstand and lowstand deposits display very irregular patterns in the isotope curves that are difficult to correlate from one section to the other.

Strontium, Mg, Na, Fe and Mn contents in the Gorges du Pichoux and Péry-Reuchenette sections are listed in Tables 2 and 3, respectively. Strontium contents vary from 37 to 226 ppm in the Gorges du Pichoux section, and from 93 to 219 ppm in the Péry-Reuchenette section. Magnesium contents range from 1052 to 8839 ppm in the Gorges du Pichoux section, and from 516 to 17539 ppm in the Péry-Reuchenette section. Only the samples from the Gorges du Pichoux section include Na, whose contents vary from 113 to 283 ppm. Iron contents fluctuate from 138 to 626 ppm in the Gorges du Pichoux section, and from 0 to 345 ppm in the Péry-Reuchenette section. Manganese contents range from 40 to 122 ppm in the Gorges du Pichoux section, and from 18 to 90 ppm in the Péry-Reuchenette section.

All samples investigated with cathodoluminescence microscopy are luminescent (Fig. 5). They show yellow to orange and orange to red homogeneous luminescence. Most bioclasts show the same colour as the matrix. Iron oxides and cements tend to be brown to black.

5. Discussion

5.a. General carbon- and oxygen-isotopic trends in the Kimmeridgian

The end of the second-order transgression (second-order maximum flooding), which characterizes the Eudoxus zone in the Tethyan realm (Fig. 2), coincides with the MFD of the third large-scale sequence. There,

https://doi.org/10.1017/S0016756810000518 Published online by Cambridge University Press

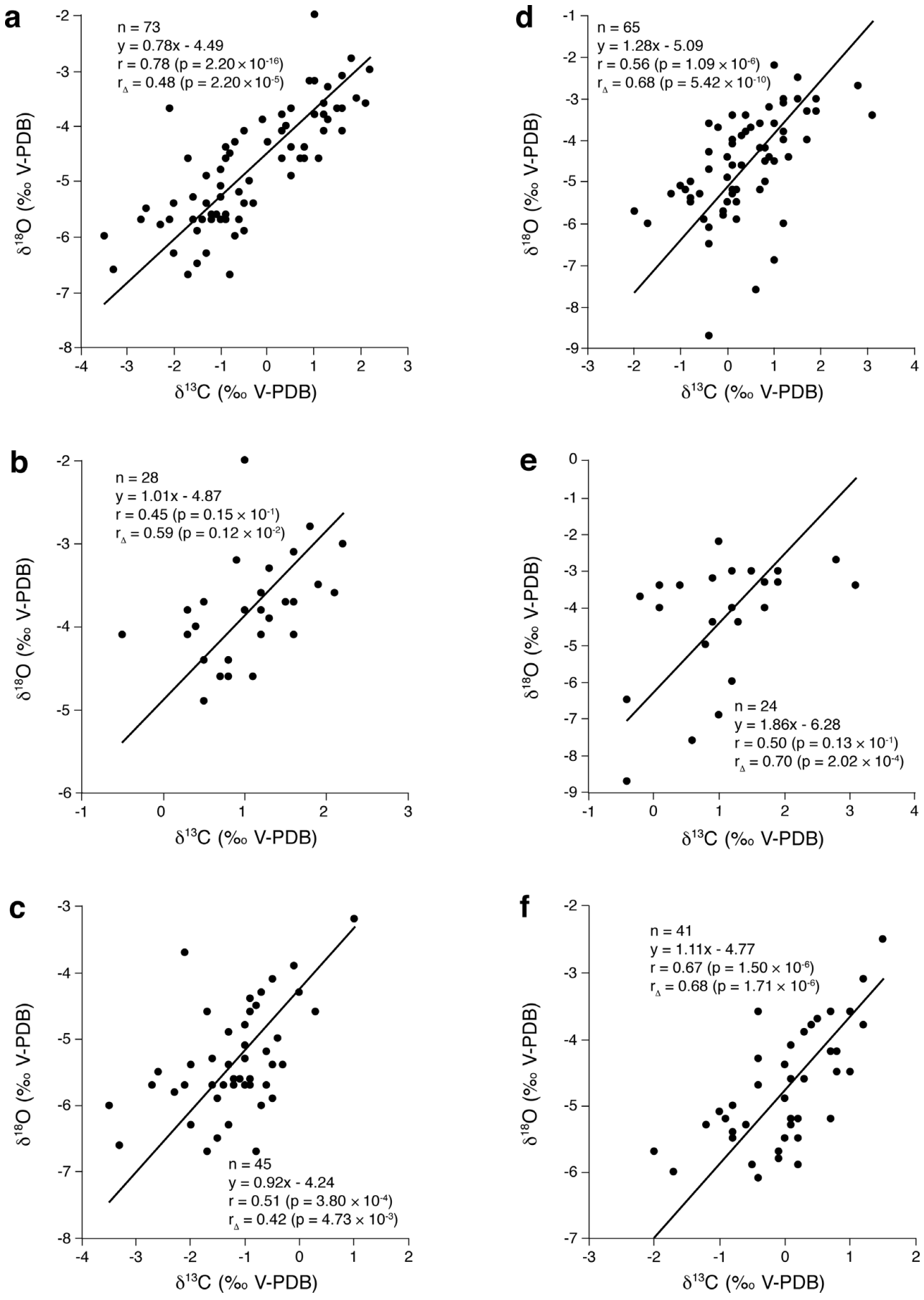

Figure 4. ($\delta^{13}C$, $\delta^{18}O$) scatter diagrams for: (a) the whole Gorges du Pichoux section, (b) the lower part (from Pi 17 to Pi 107) and (c) the upper part (from Pi 108 to Pi 234) of the Gorges du Pichoux section; (d) the whole Péry-Reuchenette section, (e) the lower part (from Re 24.4 to Re 29.20) and (f) the upper part (from Re 29.21 to Re 10.5) of the Péry-Reuchenette section. $\delta^{13}C$ and $\delta^{18}O$ values are interrelated variables whatever the studied section and interval.

https://doi.org/10.1017/S0016756810000518 Published online by Cambridge University Press

Table 2. Sr, Mg, Na, Fe and Mn contents (ppm) in the Gorges du Pichoux samples

Samples	Sr	Mg	Na	Fe	Mn	Samples	Sr	Mg	Na	Fe	Mn	Samples	Sr	Mg	Na	Fe	Mn
Pi 17	129	2075	161	329	49	Pi 96	131	2782	221	368	93	Pi 173	37	1340	130	217	78
Pi 20	105	2449	193	327	47	Pi 99	124	2619	206	302	91	Pi 177	115	3038	241	323	121
Pi 22	102	2408	199	372	49	Pi 104	172	2983	246	533	108	Pi 183	47	1427	159	299	88
Pi 24	116	2662	264	429	55	Pi 108	67	1935	128	306	45	Pi 190	46	1700	200	214	98
Pi 26	84	1991	156	273	40	Pi 110	45	1052	124	353	43	Pi 195	48	1267	146	242	92
Pi 32	134	2745	230	310	41	Pi 113	67	1145	138	320	49	Pi 199	60	1909	167	286	79
Pi 34	118	2212	229	420	42	Pi 115′	151	2313	186	408	74	Pi 203	47	1359	142	248	92
Pi 40	111	2261	197	608	62	Pi 116	110	2391	204	402	73	Pi 208	47	1347	125	289	81
Pi 43	146	2813	248	423	71	Pi 120	226	3231	235	626	67	Pi 213	47	1382	120	237	118
Pi 48	146	3003	283	511	71	Pi 122	195	4485	235	457	69	Pi 217	39	1110	113	253	73
Pi 50	147	2956	260	492	65	Pi 124	162	4294	203	402	71	Pi 221	66	1305	124	138	75
Pi 53	132	2656	202	464	67	Pi 128	67	1162	114	217	119	Pi 225	72	1285	140	201	105
Pi 58	93	1793	148	382	58	Pi 137	67	1364	159	239	102	Pi 228	68	1344	114	223	104
Pi 60	109	2061	159	375	56	Pi 142	61	1311	147	222	103	Pi 231	73	1357	138	197	92
Pi 66	111	1992	173	374	55	Pi 145	80	1547	148	289	119	Pi 234	87	1645	166	203	98
Pi 71	113	2956	208	351	64	Pi 147	51	1419	127	251	85						
Pi 77	169	8839	262	606	70	Pi 149	61	1229	141	219	75	Minimum	37	1052	113	138	40
Pi 80	153	2381	182	393	46	Pi 152	44	1126	162	213	91	Maximum	226	8839	283	626	122
Pi 89	207	3555	209	539	100	Pi 158	69	1597	140	234	102	Mean	100	2193	178	337	78
Pi 90	144	2564	195	367	84	Pi 169	58	1447	133	237	122	σ	47	1219	46	116	23

Analyses were performed in collaboration with Laurent Emmanuel at the University of Dijon. σ is standard deviation.

Table 3. Sr, Mg, Fe and Mn contents (ppm) in the Péry-Reuchenette samples

Samples	Sr	Mg	Fe	Mn	Samples	Sr	Mg	Fe	Mn	Samples	Sr	Mg	Fe	Mn
Re 24.4	136	1690	142	18	Re 29.20	166	1692	0	33	Re 23.10	115	599	0	59
Re 27.6	146	1996	192	22	Re 29.21	139	1176	43	22	Re 23.13	110	812	0	34
Re 27.9	145	1945	107	23	Re 29.22	143	1154	36	32	Re 23.15	153	940	0	44
Re 27.15	158	4118	198	27	Re 29.25	152	1123	0	35	Re 23.17	124	606	0	39
Re 27.17	167	1890	143	26	Re 29.26	194	1231	0	39	Re 23.20	117	516	0	26
Re 27.19	111	1488	81	18	Re 25.4	200	1754	0	21	Re 9.1	121	843	0	27
Re 27.21	104	2411	139	34	Re 25.9	157	836	0	34	Re 9.2	123	927	0	27
Re 27.24	143	1749	87	30	Re 25.11	189	1367	0	37	Re 9.3	105	624	0	42
Re 27.25	144	1472	89	29	Re 25.12	164	1425	1	36	Re 9.5	100	909	0	24
Re 27.27	151	2029	161	44	Re 25.14	157	1745	0	34	Re 9.6	102	707	0	28
Re 27.29	129	1828	87	54	Re 25.15	165	1519	0	33	Re 9.7	107	663	0	26
Re 27.32	187	3219	96	65	Re 25.17	132	1164	0	47	Re 9.9	114	610	0	23
Re 27.35	149	10931	293	57	Re 25.18	189	3419	0	36	Re 9.10	101	742	0	39
Re 27.36	172	6726	181	40	Re 30.2	148	2848	0	22	Re 10.2	126	846	0	36
Re 27.38	119	17539	345	54	Re 30.5	93	1324	0	27	Re 10.4	130	770	0	54
Re 29.1	138	1929	71	52	Re 30.6	219	1473	0	31	Re 10.5	173	713	0	34
Re 29.5	180	2522	25	90	Re 30.8	128	1399	0	33					
Re 29.7	195	5302	0	81	Re 30.10	122	2048	0	38	Minimum	93	516	0	18
Re 29.9	170	2189	0	63	Re 30.13	137	1223	0	30	Maximum	219	17539	345	90
Re 29.11	183	2419	0	60	Re 23.1	99	14648	0	57	Mean	144	2314	41	40
Re 29.13	178	3675	8	64	Re 23.4	124	892	0	65	σ	30	3031	76	16
Re 29.16	169	2473	0	56	Re 23.6	126	790	0	46					
Re 29.17	171	3141	26	62	Re 23.8	137	705	0	39					

Analyses were performed at the Department of Earth Sciences of the University of Oxford. σ is standard deviation.

both studied sections exhibit the most-open marine facies, the thickest beds, and relatively negative $\delta^{13}C$ and $\delta^{18}O$ values (Fig. 3). The general decrease in the isotopic values from the base of the studied interval to the second-order MFD coincides with this long-term transgressive trend. The high-resolution Tethyan-to-boreal correlation performed by Colombié & Rameil (2007) shows that the second-order MFD in the Swiss Jura corresponds to a positive shift in $\delta^{13}C$ (Fig. 6) in bulk organic matter from the Kimmeridge Clay Formation (KCF) of southern England (Morgans-Bell *et al.* 2001). However, the enhanced $\delta^{13}C_{TOC}$ values in the KCF mostly correlate with enhanced TOC values that probably result from enhanced preservation of carbohydrates through sulphurization (van Dongen, Schouten & Sinninghe Damste, 2006). They are most likely caused by a longer duration of photic zone euxinia in the depositional environment and do not reflect the overall composition of dissolved inorganic carbon in seawater. Moreover, whatever the palaeogeographical location (boreal or Tethyan), the Late Kimmeridgian is characterized by either an increase or a decrease in carbon- and oxygen-isotope ratios (Morgans-Bell *et al.* 2001; Weissert & Mohr, 1996; Jenkyns *et al.* 2002; Bartolini, Baumgartner & Guex, 1999; Bartolini, Baumgartner & Hunziker, 1996; Cecca *et al.* 2001; Gröcke *et al.* 2003; Morettini *et al.* 2002; Padden *et al.* 2002; Price & Gröcke, 2002; Price & Rogov, 2009; Riboulleau *et al.* 1998; Wierzbowski, 2004). Lastly, the compilation of $\delta^{18}O$ and $\delta^{13}C$ values from diagenetically little altered Phanerozoic fossil shells indicates a general decrease in $\delta^{18}O$ and $\delta^{13}C$

https://doi.org/10.1017/S0016756810000518 Published online by Cambridge University Press

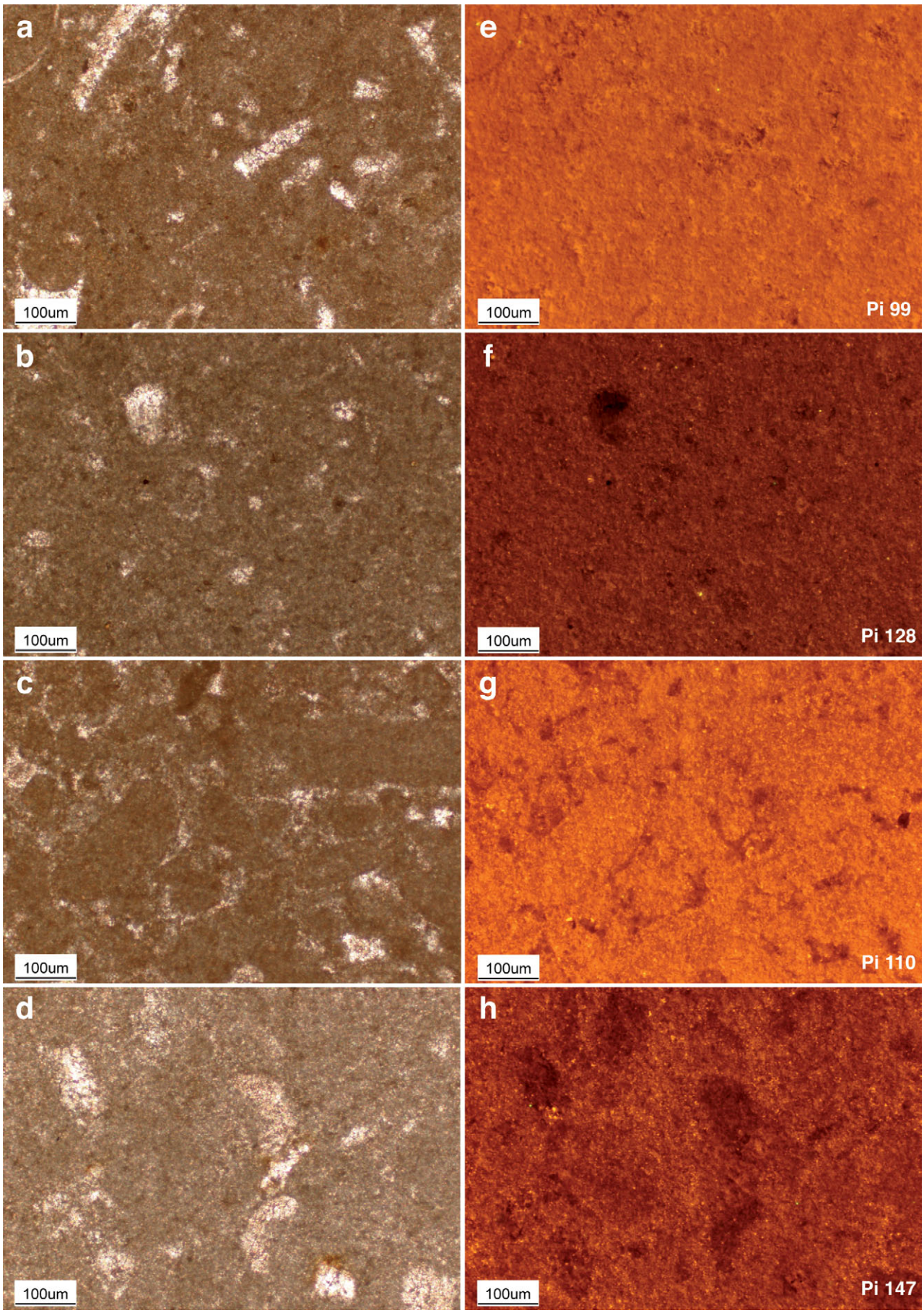

Figure 5. Plain light (a, b, c, d) and cathodoluminescence (e, f, g, h) photomicrographs of samples Pi 99 (a, e), and Pi 128 (b, f) characterizing transgressive deposits, and Pi 110 (c, g), and Pi 147 (d, h) representing maximum-flooding deposits of the Gorges du Pichoux section. Most samples are fine-grained micrites and show yellow to orange and orange to red homogeneous luminescence, which indicates that the studied samples have undergone diagenetic alteration.

https://doi.org/10.1017/S0016756810000518 Published online by Cambridge University Press

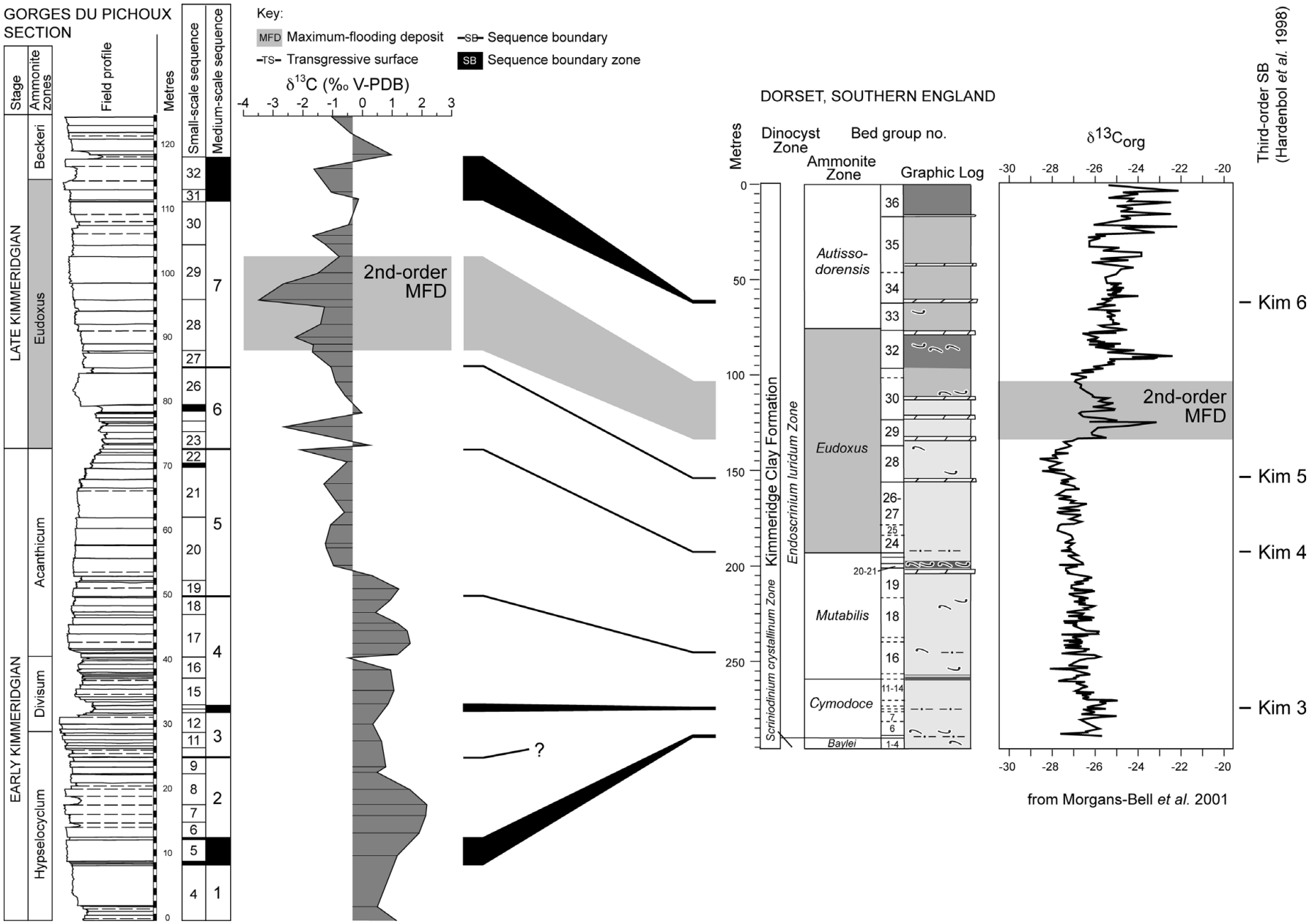

Figure 6. Correlation of carbon-isotope ratio variations between the Swiss Jura and the lower part of the Kimmeridge Clay Formation in southern England according to Colombié & Rameil (2007). The second-order MFD in the Gorges du Pichoux section, which shows the lowest $\delta^{13}C$ values, coincides with a positive shift in $\delta^{13}C$ in the Kimmeridge Clay Formation of southern England. Carbon- and oxygen-isotopic composition increases or decreases in the Late Kimmeridgian depending on geographical location, suggesting that high-resolution variations in $\delta^{13}C$ values in the Swiss Jura partly result from diagenetic alteration or changes in local environmental conditions.

Controls on $\delta^{18}O$ and $\delta^{13}C$ of ABIOTIC/BIOTIC carbonates			REFERENCES	$\delta^{18}O$	$\delta^{13}C$
PRIMARY	Fractionation of O and C isotopes	PRECIPITATION OF CARBONATES mineralogy	Patterson & Walter, 1994a; Romanek, Grossman & Morse, 1992; Swart & Eberli, 2005; Zeebe, 1999	+	+
		increasing temperature		−	
		increasing pH		−	−
		VITAL EFFECTS kinetic effects	Auclair, Joachimski & Lécuyer, 2003; Auclair *et al.* 2004; McConnaughey, 1989a; McConnaughey, 1989b	−	−
	Changes in the O and C isotopic composition of seawater	freshwater discharge	Patterson & Walter, 1994a	−	−
		VITAL EFFECTS metabolic effects	Auclair, Joachimski & Lécuyer, 2003; Auclair *et al.* 2004; Lloyd, 1962; McConnaughey, 1989a; McConnaughey *et al.* 1997; Patterson & Walter, 1994a		
		respiration			−
		photosynthesis			+
		organic matter oxidation	Joachimski, 1994; Lloyd, 1962		−
		organic matter production and burial			+
		carbonate precipitation			−
		carbonate dissolution			+
		evaporation	Patterson & Walter, 1994a	+	
		water mass "ageing"	Gomez *et al.* 2007; Holmden *et al.* 1998; Lloyd, 1962; Panchuk, Holmden & Kump, 2005; Panchuk, Holmden & Leslie, 2006; Patterson & Walter 1994a		−
DIAGENETIC		syndepositional diagenesis	Panchuk, Holmden & Leslie, 2006; Patterson & Walter, 1994b	+	+
		early meteoric diagenesis	Allan & Matthews, 1982; Brand & Veizer, 1981; Immenhauser *et al.* 2002; Immenhauser *et al.* 2003; Joachimski, 1994; Lohmann, 1988; Moore, 2001; Veizer *et al.* 1999	−	−
		burial diagenesis	Moore, 2001	−	+

Figure 7. Primary and diagenetic controls on $\delta^{13}C$ and $\delta^{18}O$ values of abiotic and biotic carbonates according to the references listed in this figure, but see also Immenhauser, Holmden & Patterson (2007), Marshall (1992), Anderson & Arthur (1983), Scholle & Arthur (1980) and Zeebe & Wolf-Gladrow (2001). Primary oxygen- and carbon-isotopic composition of carbonates depends on fractionation of oxygen and carbon isotopes during precipitation of carbonates or kinetic vital effects, or changes of the oxygen- and carbon-isotopic composition of seawater.

values during the Late Jurassic (Prokoph, Shields & Veizer, 2008; Veizer *et al.* 1999). At 150 Ma, which is approximately the age of the studied interval, mean $\delta^{18}O$ and $\delta^{13}C$ values were −0.75 ‰ and 1.7 ‰, respectively (Veizer *et al.* 1999). More recently, Prokoph, Shields & Veizer (2008) gave −1.5 ‰ for $\delta^{18}O$ and 2.8 ‰ for $\delta^{13}C$ of brachiopods. These values are consistent with those measured by Riboulleau *et al.* (1998) and Wierzbowski (2004) from belemnite rostra: $\delta^{18}O$ and $\delta^{13}C$ values varied from −1.8 to 0 ‰ and from −1.5 to 3 ‰, respectively. Most of these values are higher than the mean $\delta^{18}O$ and $\delta^{13}C$ values presented here (that is, −4.6 and 0 ‰, respectively).

Consequently, the general decrease in the carbon- and oxygen-isotopic ratios from the base of the studied interval to the second-order MFD coincides with secular changes that are expressed also on a more global scale. However, both studied sections show lower values than those measured from contemporaneous shell or whole rock samples in other basins, and high-frequency changes in $\delta^{13}C$ and $\delta^{18}O$ values that are superimposed on the general decrease in carbon- and oxygen-isotopic compositions.

Controls on the $\delta^{13}C$ and $\delta^{18}O$ values of abiotic and biotic carbonates are numerous (Fig. 7). In the following, diagenetic effects and environmental conditions will be discussed.

5.b. Diagenetic alteration

Both petrography and geochemistry can be used to detect diagenetic products (Marshall, 1992; Moore, 2001). Cement type can be diagnostic of a particular diagenetic environment. However, identical cement types may be formed in different diagenetic environments. For example, equant drusy spar cement may precipitate in near-surface meteoric environments and under deep burial conditions (Flügel, 2004).

https://doi.org/10.1017/S0016756810000518 Published online by Cambridge University Press

Moreover, most samples from the Kimmeridgian of the Swiss Jura are fine-grained micrites, in which cementation and diagenetic alteration are difficult to identify using transmitted light microscopy (Fig. 5). Therefore, attention must be paid to isotopes, trace elements and cathodoluminescence fabrics to correctly interpret the diagenetic environment.

Only early meteoric diagenesis leads to concomitant decreases in ^{18}O and ^{13}C contents of carbonates (Fig. 7) and could explain the low $\delta^{13}C$ and $\delta^{18}O$ values measured in the Kimmeridgian of the Swiss Jura. The oxygen- and carbon-isotopic compositions of meteoric cements will depend on the isotopic composition of the meteoric waters invading the sediment. The oxygen-isotopic composition of meteoric waters is strongly latitude dependent and can vary in $\delta^{18}O$ from −20 to −2 ‰ SMOW (Anderson & Arthur, 1983; Hudson, 1977). At any specific geographic site, however, the initial $\delta^{18}O$ composition of meteoric water should be relatively constant. In most meteoric environments, the prime source for the ultimate carbon-isotopic composition of meteoric diagenetic waters is soil gas and the CO_2 derived from the dissolution of marine limestones (Allan & Matthews, 1982; Lohmann, 1988). Equilibration with organically derived CO_2 with a strongly negative $\delta^{13}C$ (−25 to −16 ‰) depends on the extent of rock–water interaction. The pattern of invariant $\delta^{18}O$ combined with variable $\delta^{13}C$, termed the meteoric calcite line, serves as the baseline relative to which chemical variations characteristic of vadose-phreatic, mixed-water and spelean environments can be discriminated (Lohmann, 1988). Trace, minor and major cations are also mobilized as carbonate rock is progressively altered. Post-depositional alteration therefore leads to increases in Mn^{2+} and Fe^{2+} contents, and decreases in Sr^{2+}, Na^{+}, ^{18}O and possibly ^{13}C contents in carbonate components (Brand & Veizer, 1981). Sr^{2+} and Mn^{2+} are useful diagenetic tracers because of their widely divergent partition coefficients, their association mostly with the carbonate lattice, and their large compositional differences in marine and meteoric water (Bodine, Holland & Borcsik, 1965; Kinsman, 1969; Turekian, 1972).

Oxygen-isotope values range from −6.7 to −2 ‰ in the Gorges du Pichoux section and from −8.7 to −2.2 ‰ in the Péry-Reuchenette section (Table 1). They are lower than the literature estimates of Kimmeridgian marine carbonates, which vary between −1.85 and 0 ‰ (Riboulleau *et al.* 1998; Wierzbowski, 2004). However, carbon-isotope values range between −3.5 and 2.2 ‰ in the Gorges du Pichoux section, and between −2 and 3.1 ‰ in the Péry-Reuchenette section (Table 1). These values are close to the $\delta^{13}C$ values from Kimmeridgian marine carbonates, which range from −1.5 to 3 ‰ (Riboulleau *et al.* 1998; Wierzbowski, 2004). Low $\delta^{18}O$ values, moreover, do not coincide with low $\delta^{13}C$ values (except for sample Pi 217). Furthermore, slopes of ($\delta^{13}C$, $\delta^{18}O$) correlation lines range from 0.78 for the whole Gorges du Pichoux section to 1.86 for the lower part of the Péry-Reuchenette section (Fig. 4), suggesting that carbon- and oxygen-isotope ratios were modified in the same way. Lastly, $\delta^{18}O$ values and Sr contents are related in the Gorges du Pichoux section, while they are two independent variables in the Péry-Reuchenette section (Fig. 8).

Changes through time in $\delta^{18}O$ and $\delta^{13}C$ values are similar in both studied sections. Increases in $\delta^{18}O$ and $\delta^{13}C$ values in TD and decreases in MFD occur in two large-scale sequences. That meteoric diagenesis can have a strong influence at low relative sea level (that is, around sequence boundaries) seems only logical. However, the slopes of ($\delta^{13}C$, $\delta^{18}O$) correlation lines are 0.77 for TD and 0.53 for MFD (Fig. 9). These slopes are in accordance with those defined for the whole studied sections and their lower and upper parts (Fig. 4). Therefore, the measured isotopic signals do not imply a stronger influence of meteoric diagenesis in the shallower-water facies of TD. Also, it is difficult to conceive that meteoric diagenesis could have dominated the deeper-water facies of MFD. Lastly, the absence of pronounced subaerial exposure surfaces excludes the possibility of long-lasting and pervasive freshwater lenses affecting thick portions of the sedimentary record.

Strontium contents in the Gorges du Pichoux and Péry-Reuchenette sections (Tables 2, 3) are very low compared to Sr contents of modern micrites (Kinsman, 1969; Andrews, Christidis & Dennis, 1997; Bosence, 1995; Gischler & Zingeler, 2002; Milliman *et al.* 1993). However, manganese contents are close to those of modern lagoonal (brackish water) or freshwater carbonate sediments (Friedman, 1969), and lower than those measured in pelagic carbonates of Kimmeridgian successions (de Rafélis *et al.* 2000). In addition, (Sr, Mn) scatter diagrams performed for the Gorges du Pichoux and Péry-Reuchenette sections do not show any relationship between Sr and Mn contents (Fig. 8), and the same is true for the (Sr, Mn) distribution covering only the TD and MFD (Fig. 9).

Cathodoluminescence microscopy was applied to check diagenetic effects. Mn^{2+} is considered as the main activator of an orange-coloured luminescence, while Fe^{2+} acts as an inhibitor resulting in a dark red (dull) or no luminescence (Joachimski *et al.* 2005; Machel *et al.* 1991; Savard, Veizer & Hinton, 1995). Since Mn^{2+} is only soluble under reducing conditions, the observed orange-coloured luminescence is indicative of diagenetic stabilization under non-oxidizing conditions (probably marine burial to burial) (van Geldern *et al.* 2006).

In conclusion, there is no clear evidence that meteoric diagenesis was not responsible for the low $\delta^{18}O$ and $\delta^{13}C$ values measured in the Kimmeridgian of the Swiss Jura. Moreover, cathodoluminescence microscopy indicates that the analysed samples have undergone diagenetic alteration that uniformly affected matrix and grains and was the

https://doi.org/10.1017/S0016756810000518 Published online by Cambridge University Press

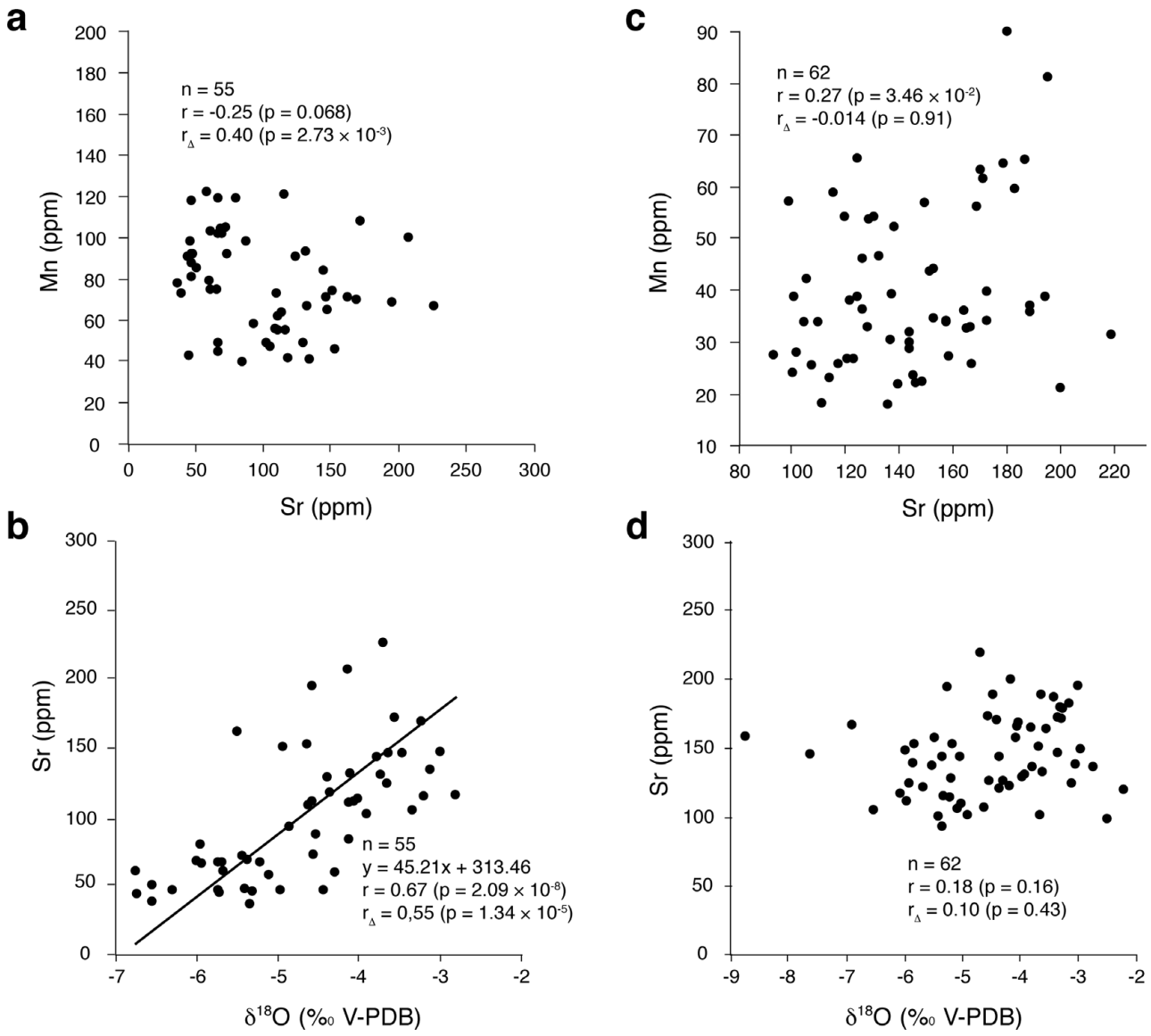

Figure 8. (Sr, Mn) and ($\delta^{18}O$, Sr) scatter diagrams for the Gorges du Pichoux (a, b) and Péry-Reuchenette (c, d) sections. $\delta^{18}O$ values and Sr contents correlate in the Gorges du Pichoux section, whereas they are two independent variables in the Péry-Reuchenette section, suggesting changes in diagenetic alteration from one section to the other.

same whatever the stratigraphic location of the studied samples.

5.c. Changes in local environmental conditions

Several controls lead to changes in the oxygen- and carbon-isotopic compositions of seawater that induce changes in the $\delta^{18}O$ and $\delta^{13}C$ values of carbonates (Fig. 7). However, only freshwater discharge results in concomitant decreases in oxygen- and carbon-isotopic compositions of carbonates. Dilution by freshwater lowers both $\delta^{13}C$ and $\delta^{18}O$ values of seawater from which marine carbonates precipitate because of depletion in ^{13}C and ^{18}O of freshwater relative to seawater (Patterson & Walter, 1994*a*). The lower part of the studied sections locally shows gyrogonites and stems of charophytes in bioturbated mudstones with fossils of euryhaline organisms (ostracodes, bivalves, miliolids). These deposits indicate ponds between channel systems that became brackish during periods of heavy rainfall (Colombié & Strasser, 2005). However, the decreasing kaolinite-to-illite ratio and quartz content, the disappearance of charophytes, and the appearance of gypsum pseudomorphs in the upper part of the studied sections indicate that climate changed from more humid to more arid at the boundary between the Early and Late Kimmeridgian (Colombié, 2002). Freshwater runoff most likely decreased from Early to Late Kimmeridgian times while salinity increased, leading to gypsum formation in the most restricted areas. Therefore, the low $\delta^{18}O$ and $\delta^{13}C$ values measured and the high-frequency changes in oxygen- and carbon-isotopic compositions observed in the Kimmeridgian of the Swiss Jura rather result from the combination of multiple factors probably controlled by high-frequency changes in

https://doi.org/10.1017/S0016756810000518 Published online by Cambridge University Press

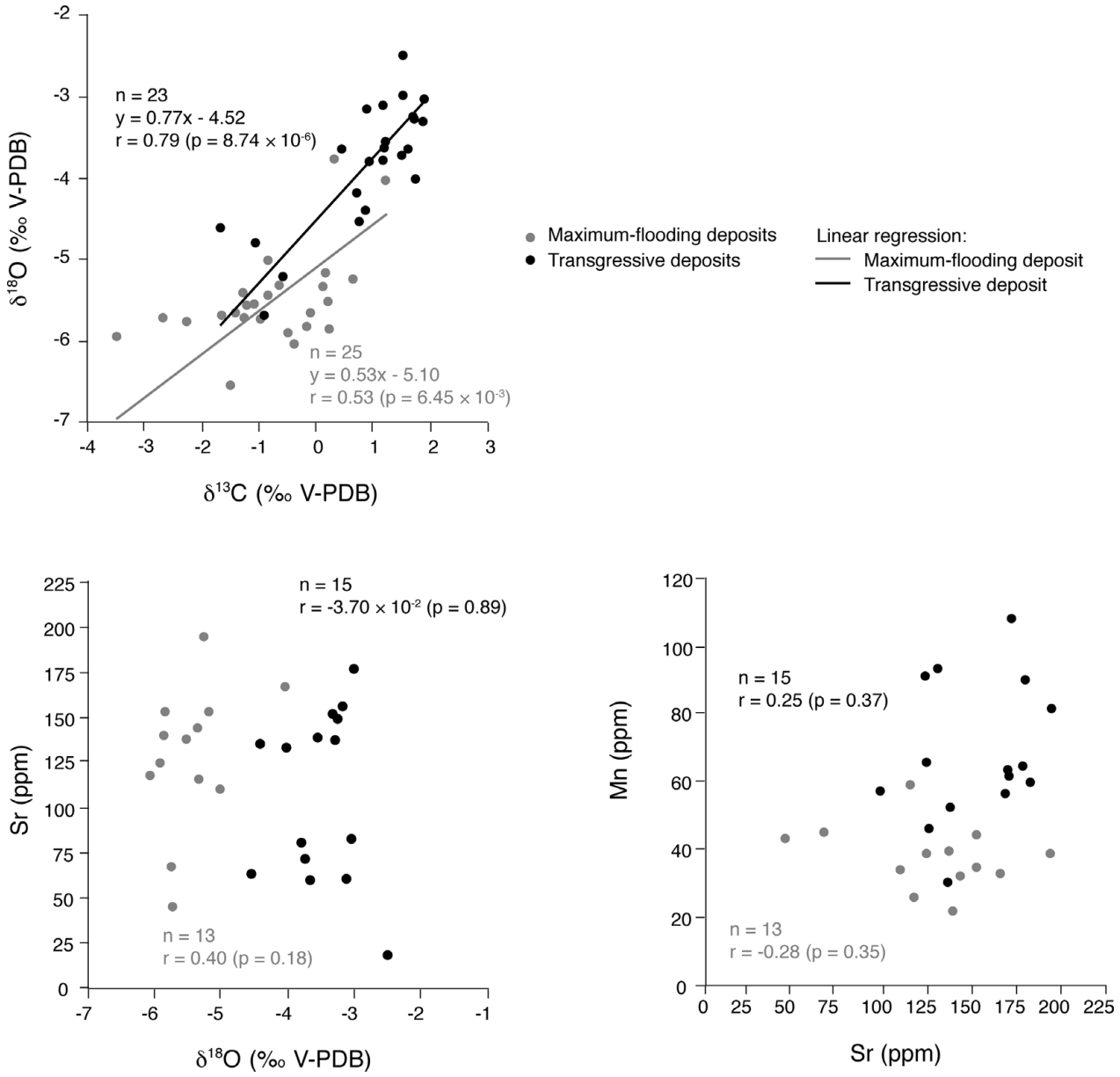

Figure 9. ($\delta^{13}C$, $\delta^{18}O$), ($\delta^{18}O$, Sr) and (Sr, Mn) scatter diagrams for large-scale transgressive (TD) and maximum-flooding (MFD) deposits. Slopes of correlation lines are in accordance with those defined for the whole and the lower and the upper parts of the studied sections. Strontium contents and $\delta^{18}O$, and Sr and Mn contents correlate neither in TD nor in MFD. The impact of diagenesis does not seem stronger in TD that are, however, shallower and more prone to diagenetic alteration than MFD.

relative sea level rather than from freshwater run-off alone.

Changes in $\delta^{13}C$ and $\delta^{18}O$ values measured in the Kimmeridgian of the Swiss Jura coincide with large-scale changes in relative sea level. Relative sea-level changes are interpreted from the evolution through time of depositional environments and bed thicknesses (Colombié, 2002; Colombié & Strasser, 2005). In a depositional sequence, the MFD correspond to the most open-marine depositional environments and to the thickest beds, which suggest the highest accommodation gain and carbonate accumulation (Colombié, 2002; Colombié & Strasser, 2005). They also coincide with decrease in $\delta^{13}C$ and $\delta^{18}O$ values.

During the Kimmeridgian, the Swiss Jura platform was characterized by tidal flats and by more or less open-marine lagoons with shoals and bioherms (Colombié & Strasser, 2005). An analysis of covariance shows that ($\delta^{13}C$, $\delta^{18}O$) correlation lines, defined for each depositional environment, are parallel (Fig. 10; Table 4), suggesting that carbon- and oxygen-isotope fractionations between carbonates and seawater were the same in each environment. ($\delta^{13}C$, $\delta^{18}O$) correlation lines defined for marsh, intertidal and open lagoonal environments in the Péry-Reuchenette section are parallel to the others (Fig. 10). However, a t-test applied to these data indicates that the corresponding $\delta^{13}C$ and $\delta^{18}O$ values are not interrelated (Table 4). This result is most likely due to scant data concerning these environments. The slopes of ($\delta^{13}C$, $\delta^{18}O$) correlation lines range from 0.34 to 1.19. These values are in accordance with those that were defined for the

https://doi.org/10.1017/S0016756810000518 Published online by Cambridge University Press

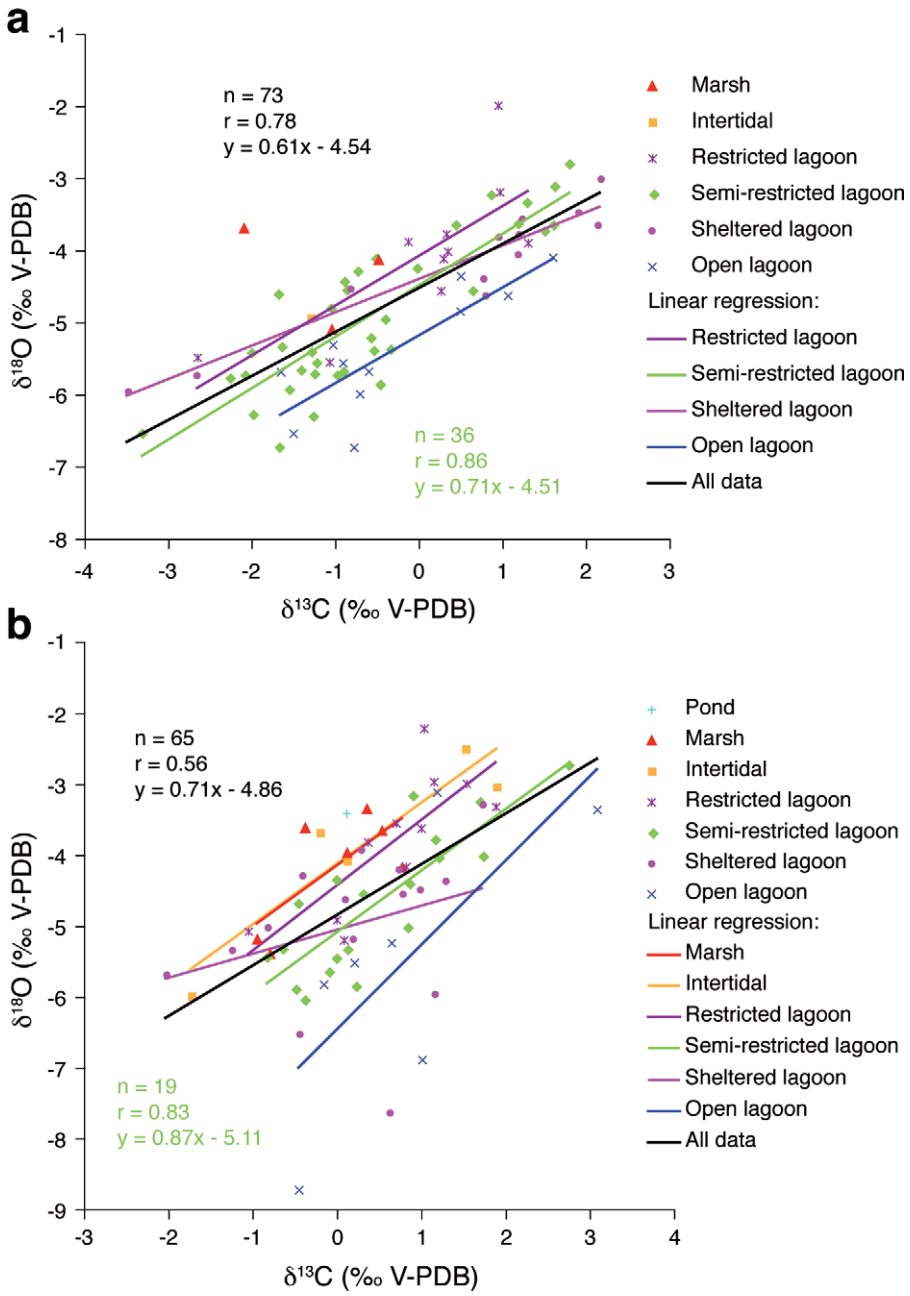

Figure 10. ($\delta^{13}C$, $\delta^{18}O$) scatter diagrams showing regression lines defined for each environment of (a) the Gorges du Pichoux and (b) the Péry-Reuchenette sections. The ($\delta^{13}C$, $\delta^{18}O$) regression lines defined for each depositional environment are parallel, suggesting that carbon- and oxygen-isotope fractionation is the same whatever the environment. These lines, however, show different *y* intercepts. This offset is probably due to water mass ageing that increases from more open-marine to more restricted environments.

whole studied sections and their lower and upper parts (Fig. 4).

For both studied sections, ($\delta^{13}C$, $\delta^{18}O$) correlation lines, defined for each depositional environment, show similar slopes but different *y* intercepts (Fig. 10). These intercepts increase from more open-marine to more restricted environments (Fig. 11). This offset is interpreted as resulting from water mass ageing that would increase towards more restricted environments. Water mass ageing describes the isolation from vigorous exchange and mixing with the ocean surface waters (Immenhauser, Holmden & Patterson, 2007; Lloyd, 1962). Broecker & Takahashi (1966) and Morse *et al.* (1984) analysed several parameters of water samples from Grand Bahama Bank. They showed that increase in water mass ageing leads to increasing salinity.

The facies model devised by Colombié (2002) and Colombié & Strasser (2005) for the Kimmeridgian of the Swiss Jura implies that salinity increased from more open-marine to more restricted, hypersaline environments. In the more proximal Gorges du Pichoux section, $\delta^{18}O$, Sr and Na are interrelated variables (Figs 7, 12). They all depend on salinity (Fritz & Katz, 1972; Jaffrezo & Renard, 1979; Land & Hoops, 1973; Veizer, 1983). In this section, decrease in

https://doi.org/10.1017/S0016756810000518 Published online by Cambridge University Press

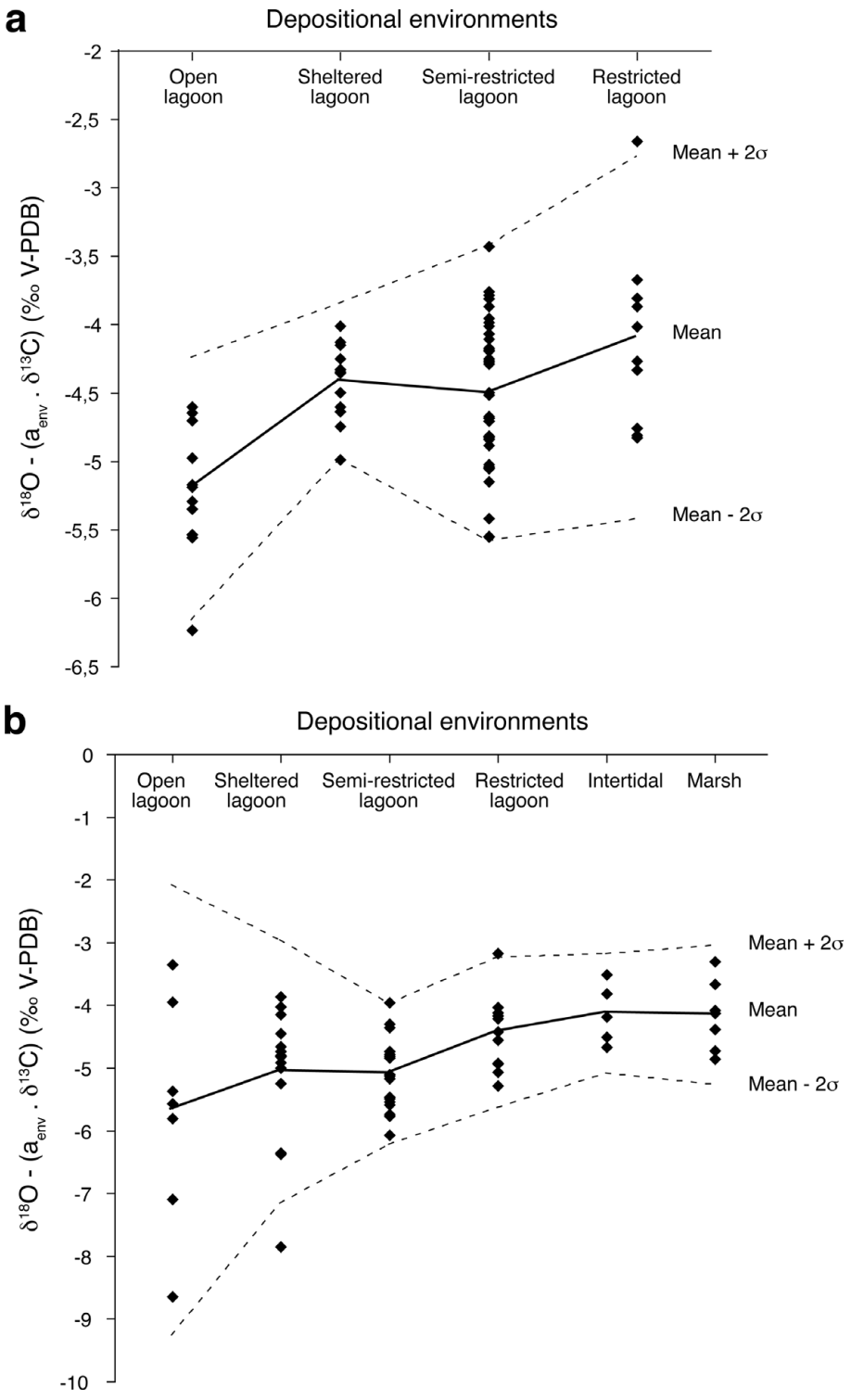

Figure 11. Rank correlation between $\delta^{18}O - (a_{env} \times \delta^{13}C)$ values and depositional environments for the (a) Gorges du Pichoux and (b) Péry-Reuchenette sections. $\delta^{18}O - (a_{env} \times \delta^{13}C)$ is the *y* intercept, and a_{env} is the slope of the ($\delta^{13}C$, $\delta^{18}O$) correlation lines that are defined for each depositional environment and listed in Table 4. Area between dashed lines represents the 95 % confidence belt. Almost all *y* intercepts lie within this confidence belt, suggesting that the increase from more open-marine to more restricted environments is significant and depends on changes in palaeoenvironmental parameters. The Tau tests performed for the Gorges du Pichoux ($\tau = 0.307$; $p = 1.9 \times 10^{-4}$) and Péry-Reuchenette ($\tau = 0.325$; $p = 1.5 \times 10^{-4}$) sections confirm that $\delta^{18}O$ values strongly depend on depositional environments.

$\delta^{18}O$ during maximum-flooding conditions can thus be explained by normal salinity in an open-marine environment, when compared to higher salinity in more restricted conditions. In the Péry-Reuchenette section, however, $\delta^{18}O$ and Sr are two independent variables (Fig. 8). Therefore, decreasing salinity alone cannot explain decreasing $\delta^{18}O$ values during MFD in the Kimmeridgian of the Swiss Jura.

https://doi.org/10.1017/S0016756810000518 Published online by Cambridge University Press

Table 4. Statistical results for each depositional environment defined in the Gorges du Pichoux and Péry-Reuchenette sections

	n	r	p (H0: r = 0)	a	b
Gorges du Pichoux					
Restricted lagoon	10	0.77	9.26×10^{-3}	0.69	−4.10
Semi-restricted lagoon	36	0.86	2.38×10^{-11}	0.71	−4.51
Sheltered lagoon	12	0.95	2.76×10^{-6}	0.46	−4.42
Open lagoon	11	0.83	1.67×10^{-3}	0.66	−5.20
Péry-Reuchenette					
Marsh	7	0.72	0.07	0.86	−4.16
Intertidal	5	0.93	0.02	0.86	−4.14
Restricted lagoon	11	0.78	4.64×10^{-3}	0.92	−4.44
Semi-restricted lagoon	19	0.83	1.30×10^{-5}	0.87	−5.11
Sheltered lagoon	15	0.31	0.25	0.34	−5.07
Open lagoon	7	0.72	0.07	1.19	−6.48

n – number of observations, r – correlation coefficient, a – slope of regression line, b – intercept of regression line.

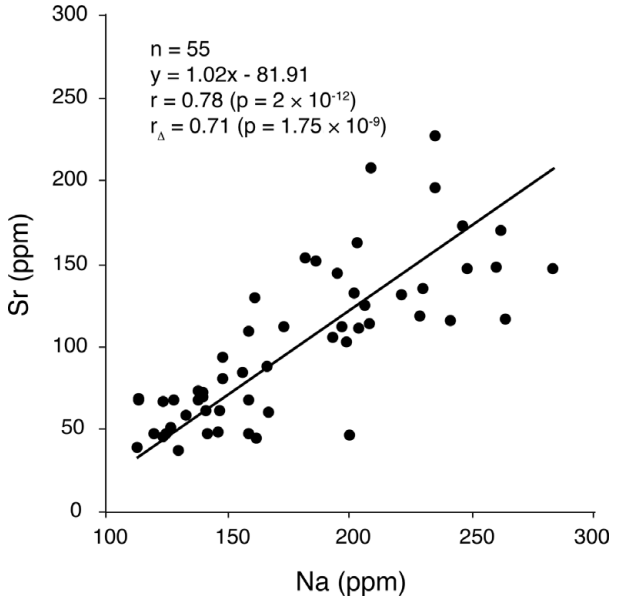

Figure 12. (Sr, Na) scatter diagram for the Gorges du Pichoux section. The correlation between Na and Sr contents may be due to a control by salinity.

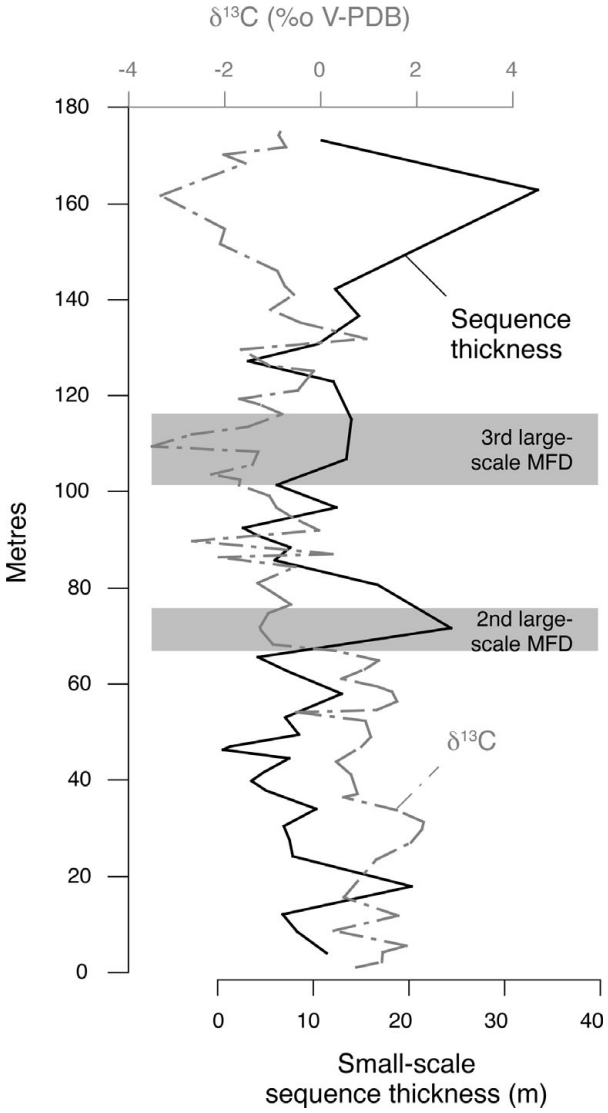

Figure 13. Changes in small-scale sequence thicknesses and $\delta^{13}C$ values in the Gorges du Pichoux section. Small-scale sequences formed within 100 ka (Colombié, 2002; Colombié & Strasser, 2005), and changes in their thicknesses reflect variations in carbonate production and accumulation rates. In the second and third large-scale MFD, negative shifts in $\delta^{13}C$ values correlate with positive shifts in sequence thicknesses, suggesting that increasing carbonate production and accumulation rates on the platform led to ^{13}C depletion in carbonates.

Broecker & Takahashi (1966) and Morse *et al.* (1984) also indicated that the mean rate of carbonate precipitation decreases with increasing water mass ageing because the waters in the region of slower carbonate precipitation are substantially less supersaturated than in areas with a high precipitation rate. In the Kimmeridgian of the Swiss Jura, small-scale sequences took 100 ka to form (Colombié, 2002; Colombié & Strasser, 2003, 2005). Changes in their thickness reflect variations in carbonate production and accumulation rates. The second and third large-scale MFD in the Gorges du Pichoux section correspond to increasing carbonate production and accumulation rates (Fig. 13). This increase in carbonate production and accumulation rates, which is due to an opening of the system, a better connection with the open ocean, and thus to decreasing water mass ageing, systematically coincides with decreasing $\delta^{13}C$ values (Fig. 13). Consequently, changes in $\delta^{13}C$ values in the Kimmeridgian of the Swiss Jura probably reflect changes in carbonate production and accumulation rates that may result from variations in residence time of waters on the platform.

Residence time of water masses, increasing with environmental restriction, may explain why $\delta^{13}C$ and $\delta^{18}O$ mean values and standard deviations are larger in the Gorges du Pichoux section, which is the more proximal section, than in the Péry-Reuchenette section, which is the more distal section (Fig. 3).

While the TD of the second large-scale sequence in both studied sections and the TD of the third large-scale sequence in the Péry-Reuchenette section show a positive shift of $\delta^{13}C$ values, the TD of the third large-scale sequence in the Gorges du Pichoux section

https://doi.org/10.1017/S0016756810000518 Published online by Cambridge University Press

is characterized by a negative shift of $\delta^{13}C$ values (Fig. 3). This decrease in $\delta^{13}C$ values coincides with an increase in carbonate production and accumulation rates (Fig. 13). This discrepancy can be explained by two separate water masses that covered the Jura platform at that time. Such compartmentalization may have been related to platform morphology, which was at least partly controlled by differential subsidence (Colombié, 2002). During highstand and lowstand conditions, compartmentalization was even more pronounced because water was generally shallower and the isolation of water bodies more likely. This explains the irregular pattern of the isotope curves in the corresponding deposits (Fig. 3).

6. Conclusions

Carbon- and oxygen-isotope analyses were performed on bulk shallow-marine carbonate samples coming from two Kimmeridgian sections located in the Swiss Jura. The comparison of the $\delta^{13}C$ and $\delta^{18}O$ records with the $\delta^{13}C$ and $\delta^{18}O$ records described from the same time interval in other basins, the use of trends in isotopic and trace-element data, as well as optical and cathodoluminescence petrography, and their combination with the sedimentological and sequence-stratigraphical interpretation of the two studied sections lead to the following conclusions:

(1) The general decrease in $\delta^{13}C$ and $\delta^{18}O$ values from the base to the top of the studied sections coincides with secular variations that are expressed on a more global scale. However, $\delta^{13}C$ and $\delta^{18}O$ values are lower than those measured from little-altered fossil shells, which reflect the general carbon- and oxygen-isotopic compositions of seawater at that time. Moreover, the Kimmeridgian carbonates of the shallow-water Jura platform show high-frequency changes in $\delta^{13}C$ and $\delta^{18}O$ values that are superimposed on the general trend.

(2) The generally more negative $\delta^{13}C$ and $\delta^{18}O$ values in the studied carbonates relative to those of the average Kimmeridgian ocean most probably result from a mix of diagenetic and local environmental effects.

(3) High-frequency changes in oxygen- and carbon-isotopic compositions might result from variations in local environmental conditions on the shallow platform, which were different from those occurring in the open ocean. Variations in $\delta^{13}C$ and $\delta^{18}O$ are interpreted to be due to changes in salinity and carbonate production and accumulation rates that result from changes in residence time of water on the platform. Platform morphology and sea-level changes modified water circulation patterns and created water masses with distinct isotopic signatures.

(4) In shallow-marine carbonates, carbon- and oxygen-isotope records can be used as a tool for long-distance stratigraphic correlations only under the condition that the origin of the isotopic signals is well understood. The correlation of the studied sections with the Kimmeridge Clay Formation of southern England has demonstrated that coeval peaks in the isotope curves can be inversed due to diagenetic alteration and different local environmental conditions.

Acknowledgements. We thank two anonymous referees for constructive criticism. Financial support for this study came from the Swiss National Science Foundation (project no. 20-56491.99 and 81FR-68839) and the French CNRS program 'ECLIPSE II'. A great part of the analyses were performed during the Ph.D. and post-doctoral research of Claude Colombié. She thanks Steve Hesselbo, from the Department of Earth Sciences of the University of Oxford in England, who hosted her for a post-doctoral year, and for his constructive comments on the last version of this manuscript. Thanks go to Maureen Padden, to Julie Cartlidge, from the Department of Earth Sciences of the University of Oxford, and to François Martineau, from the UMR CNRS 5125 of the University of Lyon 1 in France, for carbon- and oxygen-isotope analyses. Laurent Emmanuel, Benoît Vincent, and the technical staff from the University of Dijon in France and from the Department of Earth Sciences of the University of Oxford are acknowledged for trace element analyses. Thanks to Gilles Escarguel, Marie-Anne Héran and Arnaud Brayard for helping with statistical analyses. The constructive comments provided by Nicolas Olivier, Fabienne Giraud, Giovanni Aloisi, John Reijmer and Adrian Immenhauser greatly helped to improve an earlier version of this manuscript.

References

ABBINK, O., TARGARONA, J., BRINKHUIS, H. & VISSCHER, H. 2001. Late Jurassic to earliest Cretaceous palaeoclimatic evolution of the southern North Sea. *Global and Planetary Change* **30**, 231–56.

ABDI, H. 2007. Kendall rank correlation. In *Encyclopedia of Measurement and Statistics* (ed. N. J. Salkind), pp. 1–7. Thousand Oaks (CA): Sage.

ALLAN, J. R. & MATTHEWS, R. K. 1982. Isotope signatures associated with early meteoric diagenesis. *Sedimentology* **29**, 797–817.

ANDERSON, T. F. & ARTHUR, M. A. 1983. Stable isotopes of oxygen and carbon and their application to sedimentologic and paleoenvironemental problems. In *Stable Isotopes in Sedimentary Petrology* (eds M. A. Arthur, T. F. Anderson, J. Veizer & L. S. Land), pp. 1-1 to 1-151. Dallas: SEPM Short Course.

ANDREWS, J. E., CHRISTIDIS, S. & DENNIS, P. F. 1997. Assessing mineralogical and geochemical heterogeneity in the sub 63 micron size fraction of Holocene lime muds. *Journal of Sedimentary Research* **67**, 531–5.

AUCLAIR, A.-C., JOACHIMSKI, M. M. & LÉCUYER, C. 2003. Deciphering kinetic, metabolic and environmental controls on stable isotope fractionations between seawater and the shell of *Terebratalia transversa* (Brachiopoda). *Chemical Geology* **202**, 59–78.

AUCLAIR, A.-C., LÉCUYER, C., BUCHER, H. & SHEPPARD, S. M. F. 2004. Carbon and oxygen isotope composition of *Nautilus macromphalus*: a record of thermocline waters off New Caledonia. *Chemical Geology* **207**, 91–100.

BARTOLINI, A., BAUMGARTNER, P. O. & GUEX, J. 1999. Middle and Late Jurassic radiolarian palaeoecology versus carbon-isotope stratigraphy. *Palaeogeography Palaeoclimatology Palaeoecology* **145**, 43–60.

BARTOLINI, A., BAUMGARTNER, P. O. & HUNZIKER, J. 1996. Middle and Late Jurassic carbon stable-isotope

stratigraphy and radiolarite sedimentation of the Umbria-Marche Basin (Central Italy). *Eclogae geologicae Helvetiae* **89**, 811–44.

BODINE, M. W., HOLLAND, H. D. & BORCSIK, M. 1965. Coprecipitation of manganese and strontium with calcite. In *Symposium on Problems of Postmagmatic Ore Deposition*, pp. 401–6. Prague.

BOSENCE, D. W. J. 1995. Anatomy of a Recent biodetrital mud-mound, Florida Bay, USA. In *Carbonate Mud-Mounds: Their Origin and Evolution* (eds C. L. V. Monty, D. W. J. Bosence, P. H. Bridges & B. R. Pratt), pp. 439–73. Blackwell Science, International Association of Sedimentologists, Special Publication.

BRAND, U. & VEIZER, J. 1980. Chemical diagenesis of a multicomponent carbonate system – 1: trace elements. *Journal of Sedimentary Petrology* **50**, 1219–36.

BRAND, U. & VEIZER, J. 1981. Chemical diagenesis of a multicomponent carbonate system – 2: stable isotopes. *Journal of Sedimentary Petrology* **51**, 987–97.

BROECKER, W. S. & TAKAHASHI, T. 1966. Calcium carbonate precipitation on the Bahama Bank. *Journal of Geophysical Research* **71**, 1575–601.

BUONOCUNTO, F. P., SPROVIERI, M., BELLANCA, A., D'ARGENIO, B., FERRERI, V., NERI, R. & FERRUZZA, G. 2002. Cyclostratigraphy and high-frequency carbon isotope fluctuations in Upper Cretaceous shallow-water carbonates, southern Italy. *Sedimentology* **49**, 1321–37.

CECCA, F., SAVARY, B., BARTOLINI, A., REMANE, J. & CORDEY, F. 2001. The Middle Jurassic–Lower Cretaceous Rosso Ammonitico succession of Monte Inici (Trapanese domain, western Sicily): sedimentology, biostratigraphy and isotope stratigraphy. *Bulletin de la Société géologique de France* **172**, 647–60.

COLOMBIÉ, C. 2002. Sédimentologie, stratigraphie séquentielle et cyclostratigraphie du Kimméridgien du Jura suisse et du Bassin vocontien (France): relations plate-forme – bassin et facteurs déterminants. *GeoFocus* **5**, 201 pp.

COLOMBIÉ, C. & RAMEIL, N. 2007. Tethyan-to-boreal correlation in the Kimmeridgian using high-resolution sequence stratigraphy (Vocontian Basin, Swiss Jura, Boulonnais, and Dorset). *International Journal of Earth Sciences* **96**, 567–91.

COLOMBIÉ, C. & STRASSER, A. 2003. Depositional sequences in the Kimmeridgian of the Vocontian Basin (France) controlled by carbonate export from shallow-water platforms. *Geobios* **36**, 675–83.

COLOMBIÉ, C. & STRASSER, A. 2005. Facies, cycles, and controls on the evolution of a keep-up carbonate platform (Kimmeridgian, Swiss Jura). *Sedimentology* **52**, 1207–27.

DAVIS, J. C. 2002. *Statistics and Data Analysis in Geology, 3rd ed*. John Wiley & Sons.

DE RAFÉLIS, M., RENARD, M., EMMANUEL, L. & DURLET, C. 2000. Apport de la cathodoluminescence à la connaissance de la spéciation du manganèse dans les carbonates pélagiques. *Comptes Rendus de l'Académie des Sciences de Paris* **330**, 391–8.

ENOS, P. & SAWATSKY, L. H. 1981. Pore networks in Holocene carbonate sediments. *Journal of Sedimentary Petrology* **51**, 961–85.

FLÜGEL, E. 2004. *Microfacies of carbonate rocks: analysis, interpretation and application*. Springer.

FRIEDMAN, G. M. 1969. Trace elements as possible environmental indicators in carbonate sediments. In *Depositional Environments in Carbonate Rocks* (ed. G. M. Friedman), pp. 193–8. Tulsa, Oklahoma, USA: SEPM Special Publication.

FRITZ, P. & KATZ, A. 1972. The sodium distribution of dolomite crystals. *Chemical Geology* **10**, 237–44.

GISCHLER, E. & ZINGELER, D. 2002. The origin of carbonate mud in isolated carbonate platforms of Belize, Central America. *International Journal of Earth Sciences* **91**, 1054–70.

GLUMAC, B. & WALKER, K. R. 1998. A late Cambrian positive carbon-isotope excursion in the southern Appalachians: relation to biostratigraphy, sequence stratigraphy, environments of deposition, and diagenesis. *Journal of Sedimentary Research* **68**, 1212–22.

GOMEZ, F. J., OGLE, N., ASTINI, R. A. & KALIN, R. M. 2007. Paleoenvironmental and carbon-oxygen isotope record of Middle Cambrian carbonates (La Laja Formation) in the Argentine Precordillera. *Journal of Sedimentary Research* **77**, 826–42.

GRÖCKE, D. R., PRICE, G. D., RUFFELL, A. H., MUTTERLOSE, J. & BARABOSHKIN, E. 2003. Isotopic evidence for Late Jurassic–Early Cretaceous climate change. *Palaeogeography Palaeoclimatology Palaeoecology* **202**, 97–118.

GRÖTSCH, H. J., BILLING, I. & VAHRENKAMP, V. 1998. Carbon-isotope stratigraphy in shallow-water carbonates: implications for Cretaceous black-shale deposition. *Sedimentology* **45**, 623–34.

GYGI, R. A. 1995. Datierung von Seichtwassersedimenten des Späten Jura in der Nordwestschweiz mit Ammoniten. *Eclogae geologicae Helvetia* **88**, 1–58.

GYGI, R. A. & PERSOZ, F. 1986. Mineralostratigraphy, litho- and biostratigraphy combined in correlation of the Oxfordian (Late Jurassic) formations of the Swiss Jura range. *Eclogae geologicae Helvetiae* **79**, 385–454.

HALLAM, A. 1984. Continental humid and arid zones during the Jurassic and Cretaceous. *Palaeogeography Palaeoclimatology Palaeoecology* **47**, 195–223.

HALLAM, A. 1985. A review of Mesozoic climates. *Journal of the Geological Society, London* **142**, 433–45.

HARDENBOL, J., THIERRY, J., FARLEY, M. B., JACQUIN, T., DE GRACIANSKY, P.-C. & VAIL, P. R. 1998. Jurassic chronostratigraphy. In *Mesozoic and Cenozoic Sequence Stratigraphy of European Basins* (eds P.-C. de Graciansky, J. Hardenbol, T. Jacquin & P. R. Vail). SEPM Special Publication no. 60.

HOLMDEN, C., CREASER, R. A., MUEHLENBACHS, K., LESLIE, S. A. & BERGSTRÖM, S. M. 1998. Isotopic evidence for geochemical decoupling between ancient epeiric seas and bordering oceans: implications for secular curves. *Geology* **26**, 567–70.

HUDSON, J. D. 1977. Stable isotopes and limestone lithification. *Journal of the Geological Society, London* **133**, 637–60.

IMMENHAUSER, A., DELLA PORTA, G., KENTER, J. A. M. & BAHAMONDE, J. R. 2003. An alternative model for positive shifts in shallow-marine carbonate $\delta^{13}C$ and $\delta^{18}O$. *Sedimentology* **50**, 953–9.

IMMENHAUSER, A., HOLMDEN, C. & PATTERSON, W. P. 2007. Interpreting the carbon-isotope record of ancient epeiric seas: lessons from the Recent. In *Dynamics of Epeiric Seas* (eds B. R. Pratt & C. Holmden), pp. 137–74. Geological Association of Canada, Special Paper no. 48.

IMMENHAUSER, A., KENTER, J. A. M., GANSSEN, G., BAHAMONDE, J. R., VAN VLIET, A. & SAHER, M. H. 2002. Origin and significance of isotope shifts in Pennsylvanian carbonates (Asturias, NW Spain). *Journal of Sedimentary Research* **72**, 82–92.

JAFFREZO, M. & RENARD, M. 1979. Eléments en traces de calcaires à Dasycladales et Charophytes. In *Second International Symposium on Fossil Algae* (eds A. F. Poignant & R. Deloffre), pp. 639–49. New York,

Oxford: Elsevier, Bulletin du Centre de Recherches Exploration-Production Elf-Aquitaine, Introduction to Marine Micropaleontology.

JENKYNS, H. C., JONES, C. E., GRÖCKE, D. R., HESSELBO, S. P. & PARKINSON, D. N. 2002. Chemostratigraphy of the Jurassic System: applications, limitations and implications for palaeoceanography. *Journal of the Geological Society, London* **159**, 351–78.

JOACHIMSKI, M. M. 1994. Subaerial exposure and deposition of shallowing-upward sequences: evidence from stable isotopes of Purbeckian peritidal carbonates (basal Cretaceous), Swiss and French Jura Mountains. *Sedimentology* **41**, 805–24.

JOACHIMSKI, M. M., SIMON, L., VAN GELDERN, R. & LÉCUYER, C. 2005. Boron isotope geochemistry of Paleozoic brachiopod calcite: implications for a secular change in the boron isotope geochemistry of seawater over the Phanerozoic. *Geochimica et Cosmochimica Acta* **69**, 4035–44.

KENDALL, M. G. & GIBBONS, J. D. 1990. *Rank Correlation Methods, 5th ed*. London: Edward Arnold.

KINSMAN, D. J. J. 1969. Interpretation of Sr^{2+} concentrations in carbonate minerals and rocks. *Journal of Sedimentary Petrology* **39**, 486–508.

KRULL, E. S., LEHRMANN, D. J., DRUKE, D., KESSEL, B., YU, Y. Y. & LI, R. 2004. Stable carbon isotope stratigraphy across the Permian–Triassic boundary in shallow marine carbonate platforms, Nanpanjiang Basin, south China. *Palaeogeography Palaeoclimatology Palaeoecology* **204**, 297–315.

LAND, L. S. & HOOPS, G. K. 1973. Sodium in carbonate sediments and rocks: a possible index to the salinity of diagenetic solutions. *Journal of Sedimentary Petrology* **43**, 614–17.

LLOYD, R. M. 1962. Variations in the oxygen and carbon isotope ratios of Florida Bay mollusks and their environmental significance. *Journal of Geology* **72**, 84–111.

LOHMANN, K. C. 1988. Geochemical patterns of meteoric diagenetic systems and their application to studies of paleokarst. In *Paleokarst* (eds N. P. James & P. W. Choquette), pp. 58–80. Springer-Verlag.

MACHEL, H. G., MASON, R. A., MARIANO, A. N. & MUCCI, A. 1991. Causes and emission of luminescence in calcite and dolomite. In *Luminescence Microscopy: Quantitative and qualitative aspects* (eds C. E. Barker & D. C. Kopp), pp. 9–25. SEPM Short Course.

MAGARITZ, M. 1983. Carbon and oxygen isotope composition of recent and ancient coated grains. In *Coated Grains* (ed. T. M. Peryt), pp. 27–30. Berlin: Springer-Verlag.

MARSHALL, J. D. & MIDDLETON, P. D. 1980. Changes in marine isotopic composition and the late Ordovician glaciation. *Journal of the Geological Society, London* **147**, 1–4.

MARSHALL, J. D. 1992. Climatic and oceanographic isotopic signals from the carbonate rock record and their preservation. *Geological Magazine* **129**, 143–60.

MCCONNAUGHEY, T. 1989*a*. ^{13}C and ^{18}O isotopic disequilibrium in biological carbonates: I. Patterns. *Geochimica et Cosmochimica Acta* **53**, 151–62.

MCCONNAUGHEY, T. 1989*b*. ^{13}C and ^{18}O isotopic disequilibrium in biological carbonates: II. In vitro simulation of kinetic isotope effects. *Geochimica et Cosmochimica Acta* **53**, 163–71.

MCCONNAUGHEY, T., BURDETT, J., WHELAN, J. F. & PAULL, C. K. 1997. Carbon isotopes in biological carbonates: respiration and photosynthesis. *Geochimica et Cosmochimica Acta* **61**, 611–22.

MEYER, C. & PITTMAN, J. G. 1994. A comparison between the Brontopodus ichnofacies of Portugal, Switzerland and Texas. *Gaia* **10**, 125–33.

MILLIMAN, J. D., FREILE, D., STEINEN, R. P. & WILBER, R. J. 1993. Great Bahama Bank aragonitic muds: mostly inorganically precipitated, mostly exported. *Journal of Sedimentary Petrology* **63**, 589–95.

MOORE, C. H. 2001. *Carbonate Reservoirs: Porosity evolution and diagenesis in a sequence stratigraphic framework*. Elsevier.

MORETTINI, E., SANTANTONIO, M., BARTOLINI, A. & CECCA, F., BAUMGARTNER, P. O. & HUNZIKER, J. C. 2002. Carbon isotope stratigraphy and carbonate production during the Early–Middle Jurassic: examples from the Umbria–Marche–Sabina Apennines (central Italy). *Palaeogeography Palaeoclimatology Palaeoecology* **184**, 251–73.

MORGANS-BELL, H. S., COE, A. L., HESSELBO, S. P., JENKYNS, H. C., WEEDON, G. P., MARSHALL, J. E. A., TYSON, R. V. & WILLIAMS, C. J. 2001. Integrated stratigraphy of the Kimmeridge Clay Formation (Upper Jurassic) based on exposures and boreholes in south Dorset, UK. *Geological Magazine* **138**, 511–39.

MORSE, J. W., MILLERO, F. J., THURMOND, V., BROWN, E. & OSTLUND, H. G. 1984. The carbonate chemistry of Grand Bahama Bank waters: after 18 years another look. *Journal of Geophysical Research* **89**, 3604–14.

PADDEN, M., WEISSERT, H., FUNK, H., SCHNEIDER, S. & GANSNER, C. 2002. Late Jurassic lithological evolution and carbon-isotope stratigraphy of the western Tethys. *Eclogae geologicae Helvetiae* **95**, 333–46.

PANCHUK, K. M., HOLMDEN, C. & KUMP, L. R. 2005. Sensitivity of the epeiric sea carbon isotope record to local-scale carbon cycle processes: tales from the Mohawkian Sea. *Palaeogeography Palaeoclimatology Palaeoecology* **228**, 320–37.

PANCHUK, K. M., HOLMDEN, C. E. & LESLIE, S. A. 2006. Local controls on carbon cycling in the Ordovician midcontinent region of North America, with implications for carbon isotope secular curves. *Journal of Sedimentary Research* **76**, 200–11.

PATTERSON, W. P. & WALTER, L. M. 1994*a*. Depletion of ^{13}C in seawater CO_2 on modern carbonate platforms: significance for the carbon isotopic record of carbonates. *Geology* **22**, 885–8.

PATTERSON, W. P. & WALTER, L. M. 1994*b*. Syndepositional diagenesis of modern platform carbonates: evidence from isotopic and minor element data. *Geology* **22**, 127–30.

PRICE, G. D. 1999. The evidence and implications of polar ice during the Mesozoic. *Earth-Science Reviews* **48**, 183–210.

PRICE, G. D. & GRÖCKE, D. R. 2002. Strontium-isotope stratigraphy and oxygen- and carbon-isotope variation during the Middle Jurassic–Early Cretaceous of the Falkland Plateau, South Atlantic. *Palaeogeography Palaeoclimatology Palaeoecology* **183**, 209–22.

PRICE, G. D. & ROGOV, M. A. 2009. An isotopic appraisal of the Late Jurassic greenhouse phase in the Russian Platform. *Palaeogeography Palaeoclimatology Palaeoecology* **273**, 41–9.

PROKOPH, A., SHIELDS, G. A. & VEIZER, J. 2008. Compilation and time-series analysis of a marine carbonate $\delta^{18}O$, $\delta^{13}C$, $^{87}Sr/^{86}Sr$ and $\delta^{34}S$ database through Earth history. *Earth-Science Reviews* **87**, 113–33.

RAMEIL, N. 2005. Carbonate sedimentology, sequence stratigraphy, and cyclostratigraphy of the Tithonian in the Swiss and French Jura Mountains. *GeoFocus* **13**, 1–246.

RENARD, M. & BLANC, P. 1971. Mise au point d'un protocole expérimental pour le dosage des éléments traces (V, Cr, Mn, Ni, Sr, Mo) par absorption atomique. *Comptes Rendus de l'Académie des Sciences de Paris* **272**, 2285–8.

RIBOULLEAU, A., BAUDIN, F., DAUX, V., HANTZPERGUE, P., RENARD, M. & ZAKHAROV, V. 1998. Evolution de la paléotempératures des eaux de la plate-forme russe au cours du Jurassique supérieur. *Comptes Rendus de l'Académie des Sciences de Paris, Sciences de la Terre et des Planètes* **326**, 239–46.

RICHEBOIS, G. 1990. *Dosage de quelques éléments traces dans les eaux naturelles et les roches carbonatées. Application à l'étude géochimique de la coupe du Kef (Tunisie)*. Diplôme d'Etudes Supérieures Memoir. Paris, France: Université P.-et-M. Curie, 90 pp.

ROMANEK, C. S., GROSSMAN, E. L. & MORSE, J. W. 1992. Carbon isotopic fractionation in synthetic aragonite and calcite: effects of temperature and precipitation rate. *Geochimica and Cosmochimica Acta* **56**, 419–30.

SAVARD, M. M., VEIZER, J. & HINTON, R. H. 1995. Cathodoluminescence at low Fe and Mn concentrations: A SIMS study of zones in natural calcites. *Journal of Sedimentary Research* **A65**, 208–13.

SCHOLLE, P. A. & ARTHUR, M. A. 1980. Carbon isotope fluctuations in Cretaceous pelagic limestones: potential stratigraphic and petroleum exploration tool. *American Association of Petroleum Geologists Bulletin* **64**, 67–87.

SCHWEIGERT, G. & CALLOMON, J. H. 1997. Der *bauhini*-Faunenhorizont und seine Bedeutung fur die Korrelation zwischen tethyalem und subborealem Oberjura. *Stuttgarter Beiträge zur Naturkunde*, *Serie B* (*Geologie und Paläontologie*) **247**, 1–69.

SELLWOOD, B. W., VALDES, P. J. & PRICE, G. D. 2000. Geological evaluation of multiple general circulation model simulations of Late Jurassic palaeoclimate. *Palaeogeography Palaeoclimatology Palaeoecology* **156**, 147–60.

SOKAL, R. R. & ROHLF, F. J. 1995. *Biometry: The Principles and Practice of Statistics in Biological Research, 3rd ed*. New York: W. H. Freeman and Co.

SWART, P. K. & EBERLI, G. 2005. The nature of the $\delta^{13}C$ of periplatform sediments: Implications for stratigraphy and the global carbon cycle. *Sedimentary Geology* **175**, 115–29.

THALMANN, H. K. 1966. Zur Stratigraphie des oberen Malm im südlichen Berner und Solothurner Jura. *Mitteilungen der Naturforschenden Gesellschaft des Kantons Solothurn* **22**, 4–25.

TUREKIAN, K. K. 1972. *Chemistry of the Earth*. New York: Holt, Rinehart and Winston, Inc.; Physical Science and Technology series.

VAHRENKAMP, V. C. 1996. Carbon isotope stratigraphy of the Upper Kharaib and Shuaiba Formations: implications for the Early Cretaceous evolution of the Arabian Gulf region. *Bulletin of the American Association of Petroleum Geologists* **80**, 647–62.

VAN DONGEN, B. E., SCHOUTEN, S. & SINNINGHE DAMSTE, J. S. 2006. Preservation of carbohydrates through sulfurization in a Jurassic euxinic shelf sea: examination of the Blackstone Band TOC cycle in the Kimmeridge Clay Formation, UK. *Organic Geochemistry* **37**, 1052–73.

VAN GELDERN, R., JOACHIMSKI, M. M., DAY, J., JANSEN, U., ALVAREZ, F., YOLKIN, E. A. & MA, X.-P. 2006. Carbon, oxygen and strontium isotope records of Devonian brachiopod shell calcite. *Palaeogeography Palaeoclimatology Palaeoecology* **240**, 47–67.

VEIZER, J. 1983. Chemical diagenesis of carbonates: theory and application of trace element technique. In *Stable Isotopes in Sedimentary Petrology* (eds M. A. Arthur, T. F. Anderson, J. Veizer & L. S. Land), pp. 3-1 to 3-100. Dallas: SEPM Short Course.

VEIZER, J., ALA, D., AZMY, K., BRUCKSCHEN, P., BUHL, D., BRUHN, F., CARDEN, G. A. F., DIENER, A., EBNETH, S., GODDERIS, Y., JASPER, T., KORTE, C., PAWELLEK, F., PODLAHA, O. G. & STRAUSS, H. 1999. $^{87}Sr/^{86}Sr$, $\delta^{13}C$ and $\delta^{18}O$ evolution in Phanerozoic seawater. *Chemical Geology* **161**, 59–88.

WEISSERT, H. & MOHR, H. 1996. Late Jurassic climate and its impact on carbon cycling. *Palaeogeography Palaeoclimatology Palaeoecology* **122**, 27–43.

WEISSERT, H., LINI, A., FÖLLMI, K. & KUHN, O. 1998. Correlation of Early Cretaceous carbon isotope stratigraphy and platform drowning events: a possible link? *Palaeogeography Palaeoclimatology Palaeoecology* **137**, 189–203.

WIERZBOWSKI, H. 2004. Carbon and oxygen isotope composition of Oxfordian–Early Kimmeridgian belemnite rostra: palaeoenvironmental implications for Late Jurassic seas. *Palaeogeography Palaeoclimatology Palaeoecology* **203**, 153–68.

WIGNALL, P. B. & RUFFELL, A. H. 1990. The influence of a sudden climatic change on marine deposition in the Kimmeridgian of Northwest Europe. *Journal of the Geological Society, London* **147**, 365–71.

ZEEBE, R. E. 1999. An explanation of the effect of seawater carbonate concentration on foraminiferal oxygen isotopes. *Geochimica and Cosmochimica Acta* **63**, 2001–7.

ZEEBE, R. E. & WOLF-GLADROW, D. 2001. *CO_2 in Seawater: Equilibrium, Kinetics, Isotopes*. Amsterdam: Elsevier.

https://doi.org/10.1017/S0016756810000518 Published online by Cambridge University Press